AD-A103 804 ANALYTIC SCIENCES CORP READING MA F/G 17/7
APPLICATION OF SEMI-EMPIRICAL TD GRID CALIBRATION TO THE WEST C--ETC(U)
JUL 79 R R GUPTA DOT-CG-81-77-1785
UNCLASSIFIED TASC-TR-1119-2-1C USCG-D-29-81 NL

1 of 1
AD
A103804

END
DATE
FILMED
10-81
DTIC

Technical Report Documentation Page

1. Report No.	2. Government Accession No.	3. Recipient's Catalog No.
USCG-D-29-81	AD-A103 804	

4. Title and Subtitle	5. Report Date
Application of Semi-Empirical TD Grid Calibration to the West Coast Loran-C Chain.	Jul[redacted]979
	6. Performing Organization Code J-1119-2
7. Author(s) Radha R. Gupta	8. Performing Organization Report No. TR-1119-2-1C
9. Performing Organization Name and Address The Analytic Sciences Corporation One Jacob Way Reading, Massachusetts 01867	10. Work Unit No. (TRAIS)
	11. Contract or Grant No. DOT-CG-81-77-1785
12. Sponsoring Agency Name and Address U.S. Coast Guard Research and Development Center Groton, Connecticut 06340	13. Type of Report and Period Covered Final Report. Mar[redacted]9 — Jun[redacted]79
	14. Sponsoring Agency Code CGR&DC 2/81

15. Supplementary Notes

16. Abstract

This study demonstrates the utility of semi-empirical Loran-C time difference (TD) grid calibration techniques. Theory is employed to determine the functional dependence of TDs on range and bearing from the Loran-C chain stations. TD measurement data are then utilized to calibrate the unknown coefficients incorporated in the semi-empirical TD model. A semi-empirical model is presented for the West Coast Loran-C chain where at-sea TD measurement data in Southern California revealed large discrepancies between U.S. Coast Guard original predictions and measurements. A significant reduction in the TD errors is achieved with the semi-empirically-calibrated model relative to the U.S. Coast Guard original grid. The accuracy of the calibrated West Coast Loran-C grid is further evaluated by comparing the calibrated grid with measurements which are not used in model calibration. Results are also presented which show the sensitivity of the model accuracy to the quantity and distribution of measurement data used to calibrate the model. Guidelines are formulated to aid in the design of data collection requirements for future semi-empirical grid calibration efforts.

17. Key Words	18. Distribution Statement
Loran-C TD Grid Calibration West Coast Loran-C Chain Loran-C	

19. Security Classif. (of this report)	20. Security Classif. (of this page)	21. No. of Pages	22. Price
Unclassified	Unclassified		

METRIC CONVERSION FACTORS

Approximate Conversions to Metric Measures

Symbol	When You Know	Multiply by	To Find	Symbol
	LENGTH			
in	inches	*2.5	centimeters	cm
ft	feet	30	centimeters	cm
yd	yards	0.9	meters	m
mi	miles	1.6	kilometers	km
	AREA			
in^2	square inches	6.5	square centimeters	cm^2
ft^2	square feet	0.09	square meters	m^2
yd^2	square yards	0.8	square meters	m^2
mi^2	square miles	2.6	square kilometers	km^2
	acres	0.4	hectares	ha
	MASS (weight)			
oz	ounces	28	grams	g
lb	pounds	0.45	kilograms	kg
	short tons (2000 lb)	0.9	tonnes	t
	VOLUME			
tsp	teaspoons	5	milliliters	ml
Tbsp	tablespoons	15	milliliters	ml
fl oz	fluid ounces	30	milliliters	ml
c	cups	0.24	liters	l
pt	pints	0.47	liters	l
qt	quarts	0.95	liters	l
gal	gallons	3.8	liters	l
ft^3	cubic feet	0.03	cubic meters	m^3
yd^3	cubic yards	0.76	cubic meters	m^3
	TEMPERATURE (exact)			
°F	Fahrenheit temperature	5/9 (after subtracting 32)	Celsius temperature	°C

*1 in ≡ 2.54 (exactly). For other exact conversions and more detailed tables, see NBS Misc. Publ. 286, Units of Weights and Measures, Price $2.25, SD Catalog No. C13.10:286.

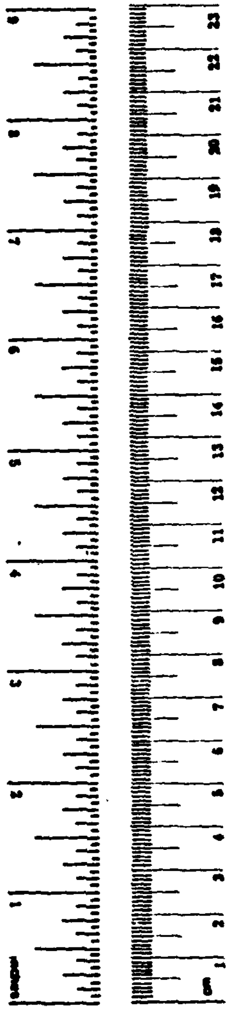

Approximate Conversions from Metric Measures

Symbol	When You Know	Multiply by	To Find	Symbol
	LENGTH			
mm	millimeters	0.04	inches	in
cm	centimeters	0.4	inches	in
m	meters	3.3	feet	ft
m	meters	1.1	yards	yd
km	kilometers	0.6	miles	mi
	AREA			
cm^2	square centimeters	0.16	square inches	in^2
m^2	square meters	1.2	square yards	yd^2
km^2	square kilometers	0.4	square miles	mi^2
ha	hectares (10,000 m^2)	2.5	acres	
	MASS (weight)			
g	grams	0.035	ounces	oz
kg	kilograms	2.2	pounds	lb
t	tonnes (1000 kg)	1.1	short tons	
	VOLUME			
ml	milliliters	0.03	fluid ounces	fl oz
l	liters	2.1	pints	pt
l	liters	1.06	quarts	qt
l	liters	0.26	gallons	gal
m^3	cubic meters	35	cubic feet	ft^3
m^3	cubic meters	1.3	cubic yards	yd^3
	TEMPERATURE (exact)			
°C	Celsius temperature	9/5 (then add 32)	Fahrenheit temperature	°F

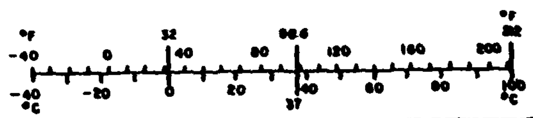

TABLE OF CONTENTS

TABLE OF CONTENTS (Continued)

LIST OF FIGURES

LIST OF TABLES

1. INTRODUCTION

1.1 BACKGROUND

Semi-empirical Loran-C time difference (TD) grid calibration techniques have been successfully employed to develop an accurate (approximately 100 nsec rms) calibrated grid for the St. Marys River Loran-C chain where groundwave signal paths exhibited "nearly homogeneous" signal propagation properties (Ref. 1). The study reported herein extends the utility of semi-empirical techniques to the development of a calibrated Loran-C grid for the Coastal Confluence Zone (CCZ) where signal paths must be considered as mixed, i.e., part land and part sea water. In particular, semi-empirical TD grid calibration techniques are applied to the West Coast Loran-C chain where the U.S. Coast Guard predictions are reported to result in large charting errors, especially in the CCZ between Los Angeles and San Diego.

1.2 WEST COAST LORAN-C CHAIN CONFIGURATION

The U.S. West Coast Loran-C chain is a long baseline chain consisting of four transmitters (Table 1.2-1) and two monitor Sites* as illustrated in Fig. 1.2-1. Time-sequenced groups of pulsed 100 kHz radiowave signals are transmitted by the four stations. The difference in time-of-arrival (TOA) of signals from two of the stations is a

*The time difference measurement data provided for this study were collected with the monitor at Point Pinos controlling the chain.

TABLE 1.2-1

WEST COAST LORAN-C CHAIN, RATE 9940(SS6), CHARACTERISTICS

STATION	COORDINATES* LATITUDE & LONGITUDE	STATION FUNCTION	EMISSION DELAY & BASELINE LENGTH (μsec)	RADIATED PEAK POWER (kW)
Fallon, Nevada	39° 33' 06.62"N 118° 49' 56.37"W	M Master		400
George, Washington	47° 03' 47.99"N 119° 44' 39.5" W	W Secondary	13796.90 2796.90	1200
Middletown, California	38° 46' 56.99"N 122° 29' 44.53"W	X Secondary	28094.50 1094.50	400
Searchlight, Nevada	35° 19' 18.18N 114° 48' 17.43"W	Y Secondary	41967.30 1967.30	500

*Based on World Geodetic System (WGS) - 1972 Datum.

measure of the difference in distance from the point of observation to each of the two stations. The locus of all points having the same observed difference in distance to a pair of stations is a hyperbola, referred to as a line-of-position (LOP). The intersection of two or more LOPs defines a user's position when compared to a chart containing a grid of calibrated LOPs.

1.3 OBJECTIVES

The objectives of the study reported herein are to:

- Develop a semi-empirical calibration technique (or model) for the West Coast Loran-C chain TD grid with an accuracy equal to or better than the current U.S. Coast Guard grid calibration procedures

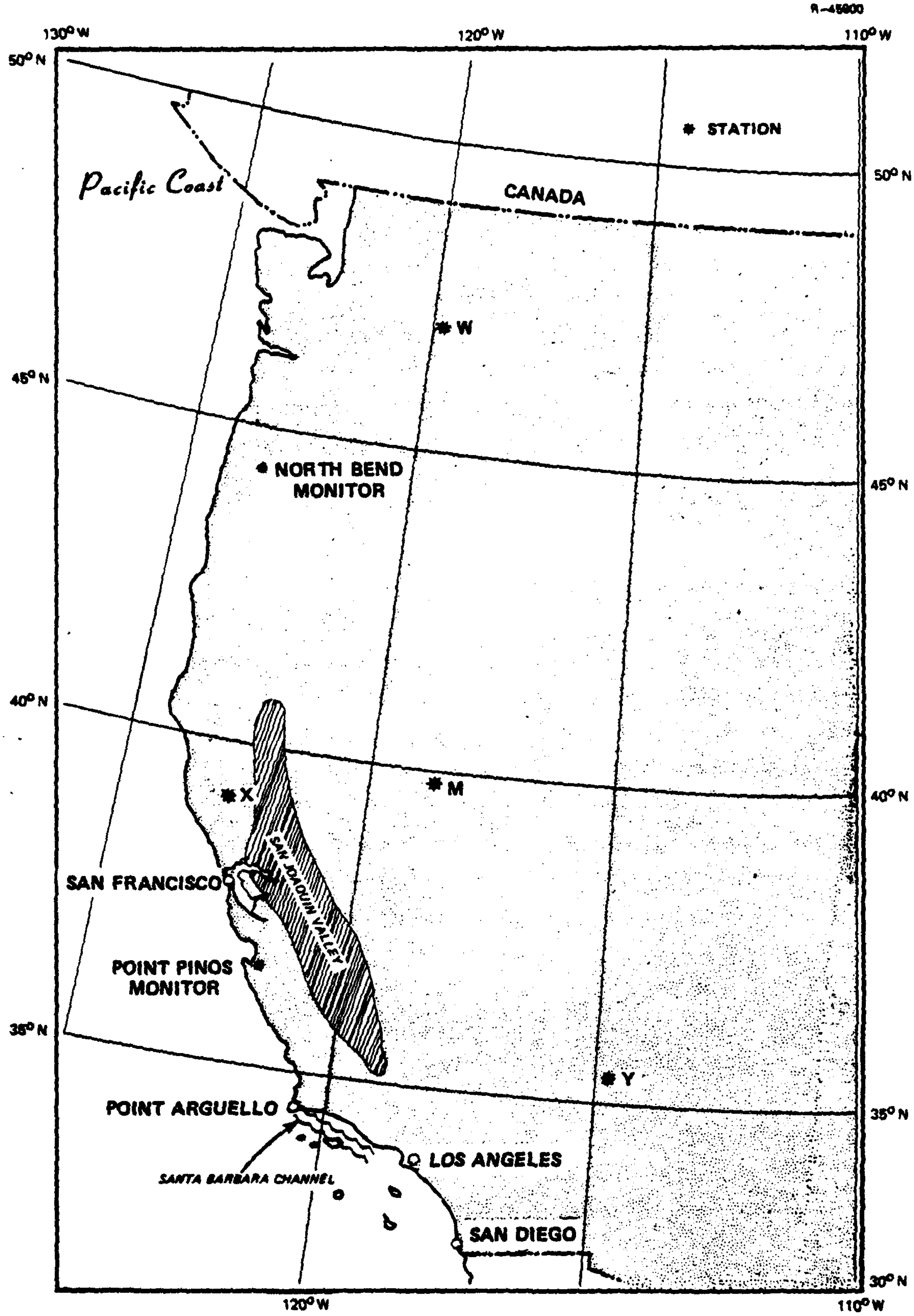

Figure 1.2-1   West Coast Loran-C Chain Configuration

- Quantify the semi-empirical calibration technique accuracy sensitivity in terms of calibration data requirements.

Based on the sensitivity analysis results, data collection guidelines are formulated for future semi-empirical grid calibration efforts. The outputs of the study include a TD grid calibration model and computed TDs at a number of at-sea data points which are not used to calibrate the grid.

1.4 TECHNICAL APPROACH

Loran-C TD measurement data are analyzed to identify dominant propagation parameter-dependent trends in the data. These trends and theory are used to establish separate polynomial structures for the land and sea water signal propagation phase delay models. Phase delay over a mixed path is then obtained by applying Millington's method (Ref. 5) which empirically combines land and sea phase delays. Data are then used in a Kalman estimation algorithm (Ref. 3) to compute the uncertain coefficients of the land and sea models of the TD grid calibration algorithm. The calibrated algorithm is used to compute TDs at each data site and the TD residuals (difference between measurement and calibrated TDs) are examined. Adjustments are then made to the TD model structure in an attempt to further reduce the residuals. This process of adjusting the model structure is repeated until the residuals agree with the expected theoretical covariance associated with the TD model. The model which exhibits the "best" performance is then selected from the several candidate models as the West Coast TD grid model. The performance of the West Coast model is further evaluated against measurements not used in calibrating the model.

Next, the sensitivity of the selected West Coast TD grid model is assessed as a function of density and quantity of the calibration data. This is accomplished by recalibrating the coefficients of the model with a subset of the data. The resulting TD residuals are evaluated for a number of uniformly distributed data densities as well as several clustered data sets. Sensitivity analysis results are used to develop general data collection requirements in terms of expected accuracy of the semi-empirically calibrated TD grid.

1.5 REPORT OVERVIEW

Theoretical basis of the semi-empirical TD grid calibration technique is described in Chapter 2. The measurement data analysis results used to identify significant trends in the data are presented in Chapter 3. The grid calibration procedure, semi-empirical models and the resulting calibrated model algorithm for the West Coast chain along with the model performance are presented in Chapter 4. The sensitivity of the calibrated model accuracy to the quantity and distribution of data is assessed in Chapter 5. Conclusions and recommendations are presented in Chapter 6. Calibrated grid model algorithm details and computed TDs at the calibration data sites appear in Appendix A.

2. THEORETICAL BASIS

2.1 INTRODUCTION

Loran-C groundwave navigation position fix accuracy is primarily dependent on a chart maker's ability to accurately compute (or determine) the expected TOA, or TD which is the difference between two TOAs, of received groundwave signals from Loran-C transmitting stations for comparison with Loran-C receiving equipment outputs. Mathematical algorithms are used in automatic equipment and manual procedures depend on the availability of accurate charts of Loran-C LOPs. In either case, accurate knowledge of the signal phase delay which establishes the true LOP is critical to Loran-C position fix accuracy.

The phase delay* of a groundwave signal is generally expressed as

$$\begin{aligned} \phi &= T + SF \\ &= \frac{n}{c} R + SF \end{aligned} \qquad (2.1\text{-}1)$$

where n is the surface refractive index, c is the speed of light in a vacuum, R is the range to the transmitting station, and SF is the phase of the secondary factor (Ref. 4). The primary signal phase delay, T, (also referred to as the primary phase delay, or primary travel time in Ref. 2) is the

---

*Phase delay, phase, propagation delay, travel time and time delay are used interchangeably throughout this report, and are expressed in units of time.

computed travel time of the Loran-C pulse over a distance equal to the transmitter-to-receiver great circle path length, accounting only for the velocity of light and the index of refraction of the atmosphere. The phase of the secondary factor (referred to as the secondary phase delay* in this report) is characterized in Ref. 4 as a correction to the primary phase delay to account for the phase delay due to signal propagation over the inhomogeneous and irregular surface of the earth. In the groundwave phase delay equation, Eq. 2.1-1, T is the dominant term and involves well-known parameters. The SF is usually an order of magnitude smaller than T but significantly more complex to determine due to the inhomogeneous electrical properties and irregularities of the earth's surface.

2.2 SF COMPUTATION TECHNIQUES

A number of analytical and empirical SF computation techniques (or models) have been reported in the literature (Refs. 4 through 7). The most commonly-used models include:

- Homogeneous/smooth path model
- Mixed Path -- Millington's empirical method
- Inhomogeneous Path -- Integral Equation approach.

---

*The secondary phase delay is equal to the sum of the Secondary Phase Factor and the Additional Secondary Factor, as defined in Ref. 2. The Secondary Phase Factor is a correction to the primary phase delay on the presumption the path is entirely sea water. The Additional Secondary Factor is a correction to the Secondary Phase Factor which accounts for an inhomogeneous earth's surface.

The homogeneous/smooth path model (Ref. 4) is useful for SF computations over a homogeneous (i.e., uniform electrical properties) signal propagation path along a smooth earth, such as an all-sea water path.

Millington's empirical approach (Ref. 5) is useful for computing the SF over a mixed (multiple-homogeneous segment) path. This approach empirically combines SFs of various homogeneous segments of a mixed path. For example, for a two segment (land and sea water) mixed path, as shown in Fig. 2.2-1, Millington's formula for the SF over the mixed path of length T_L+T_S is

$$SF(\sigma_L, \sigma_S, T_L + T_S) = \frac{1}{2} [\phi_A + \phi_B] \quad (2.2\text{-}1)$$

where

$$\phi_A = SF(\sigma_L,T_L) + [SF(\sigma_S,T_L+T_S) - SF(\sigma_S,T_L)] \quad (2.2\text{-}2)$$

$$\phi_B = SF(\sigma_S,T_S) + [SF(\sigma_L,T_L+T_S) - SF(\sigma_L,T_S)] \quad (2.2\text{-}3)$$

σ_L is the conductivity of the homogeneous land segment of the path

σ_S is the conductivity of the sea water segment of the path

$SF(\sigma,T)$ is the SF for a homogeneous path of conductivity σ and length T

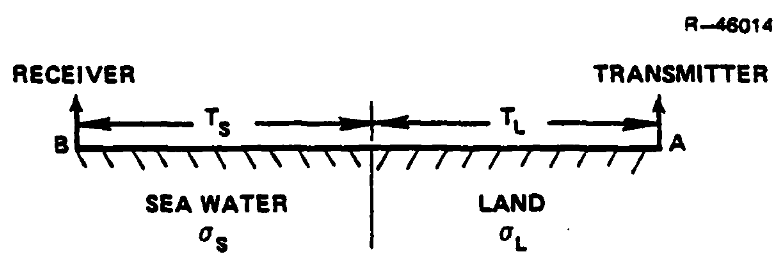

Figure 2.2-1 Two-Segment Mixed Path

The accuracy of Millington's approach is known to be good (Ref. 8) provided that reasonably accurate estimates of the homogeneous segment SFs are available.

Millington's approach has also been used by the U.S. Coast Guard to generate "effective" conductivity maps for a number of operational Loran-C chains. The map generation procedure is to use baseline and selected land TD measurement data to estimate the effective conductivity along each of the homogeneous segments of the mixed paths included in the data. Conductivities along measurement data paths are then adjusted to vary until predictions and data are in agreement within 100 nsec. Effective conductivity values are extended to regions not traversed by data paths by defining geological structures which are expected to have similar conductivities.

When the propagation path is inhomogeneous and the terrain is irregular, such that it cannot be modeled satisfactorily by either the homogeneous path or Millington's mixed path model, a more sophisticated and complicated integral equation model (Ref. 6) can be used. However, the numerical solution of the integral equation is generally expensive and cumbersome except for simple terrain irregularities and requires a relatively large computer storage capability to process all of the physiographic data characterizing the path.

In summary, analytical prediction models are useful if the modeled propagation path scenario closely approximates the "real-world" scenario and if the propagation path parameters are known. Usually, the real-world signal propagation medium of interest is far too inhomogeneous and irregular to be easily idealized. Additionally, the required propagation path parameter values are rarely known with the required precision.

2.3 SEMI-EMPIRICAL SF MODEL

The approach taken herein is to employ semi-empirical grid calibration techniques, similar to those used for calibrating the St. Marys River Loran-C chain (Ref. 1). The "physics" of the propagation medium are used to establish a functional form of the signal phase delay model and measurement data are used to calibrate the (uncertain) coefficients of the model.

A generalized semi-empirical polynomial functional form for the SF of the j^{th} station is given by

$$SF_j = SF(T_j, \beta_j) = \sum_{k=-K_1}^{K_2} A_k T_j^k + \sum_{\ell=1}^{L} [C_{j\ell} \sin \ell\beta_j + D_{j\ell} \cos \ell\beta_j] \qquad (2.2\text{-}4)$$

where

j = secondary (w, x, or y) or master (m) station

$T_j = \frac{n}{c} R_j = j^{th}$ station-to-user primary phase delay

$R_j = j^{th}$ station-to-user great-circle path length

β_j = user path bearing angle at the j^{th} station

K_1, K_2 and L are positive integers

$C_{j\ell}$ and $D_{j\ell}$ are the station-dependent coefficients of harmonic terms in the model

A_k is the range-dependent coefficient of the model which may in general be station-dependent.

The semi-empirical model can be made as complex as desired and will approach the theoretical model in the limit. However, increased complexity requires estimating an increased number of uncertain coefficients in the model, which in turn increases the amount of measurement data required. Since the primary

purpose for developing a grid calibration model is to reduce the amount of measurement data required to establish a Loran-C grid, a <u>compromise</u> must be made between model complexity and measurement data requirements. For example, for Loran-C signal propagation over a homogeneous/smooth propagation region such as an all-sea water path, the SF behavior is expected to be isotropic, i.e., independent of both path bearing angle and station location. Therefore, for this case, the semi-empirical SF model for the j^{th} station would be of the form

$$SF_j = SF(T_j) = \sum_{k=-K_1}^{K_2} A_k T_j^k \qquad (2.2\text{-}5)$$

where coefficient A_k is station-independent, i.e., it has the same numerical value for every station of the chain.

2.4 TD GRID CALIBRATION EQUATION

The true time difference (TD_i) between the time-of-arrival (TOA_i) of a groundwave signal from the i^{th} (= w, x or y) secondary station and the time-of-arrival (TOA_m) from the master station (m), is

$$\underbrace{\text{Time Difference}}_{TD_i} = \underbrace{\begin{array}{c}\text{Time-of-Arrival}\\ \text{From Secondary}\end{array}}_{TOA_i} - \underbrace{\begin{array}{c}\text{Time-of-Arrival}\\ \text{From Master}\end{array}}_{TOA_m} \qquad (2.3\text{-}1)$$

The time-of-arrivals can be expressed as

$$TOA_i = T_i + SF_i + ED_i \qquad (2.3\text{-}2)$$

$$TOA_m = T_m + SF_m \qquad (2.3\text{-}3)$$

where ED_i is the true emission delay; for the West Coast chain it is equal to the coding delay of the i^{th} secondary station of the chain plus the true baseline length. (Note, the published values of ED_i for the West Coast chain are as given in Table A.1-1.). Combining Eqs. 2.3-1 through 2.3-3, the <u>true</u> TD is given by

$$TD_i = (T_i - T_m) + (SF_i - SF_m) + ED_i \qquad (2.3\text{-}4)$$

The semi-empirical grid calibration model developed herein uses land and sea TD measurement data to calibrate the model. These measurements are corrupted by measurement noise including position reference errors, and are related to the true TD by

$$\underbrace{\begin{matrix}\text{Measured}\\ TD_i\end{matrix}}_{z_i^*} = \underbrace{\begin{matrix}\text{True}\\ TD_i\end{matrix}}_{TD_i} + \underbrace{\begin{matrix}\text{Measurement}\\ \text{Noise}\end{matrix}}_{v_i'} \qquad (2.3\text{-}5)$$

Upon substituting Eq. 2.3-4 into Eq. 2.3-5, the measured TD is

$$z_i^* = (T_i - T_m) + (SF_i - SF_m) + ED_i + v_i' \qquad (2.3\text{-}6)$$

In subsequent discussions of the TD data quality and model calibration procedure, it is convenient to transform the measured TD_i into an "Adjusted TD_i" which is defined as

$$ATD_i \equiv z_i = z_i^* - (T_i - T_m) - \overline{ED}_i \qquad (2.3\text{-}7)$$

where ED_i is the published constant emission delay (see Table 1.1-1) implemented at the secondary station. Substituting Eq. 2.3-6 into Eq. 2.3-7 gives

$$z_i = (SF_i - SF_m) + \Delta ED_i + v_i'$$
$$= (SF_i - SF_m) + v_i \tag{2.3-8}$$

where v_i ($= \Delta ED_i + v_i'$) is the total measurement error, and ΔED_i is the difference between the true and published emission delay for the i^{th} secondary station. Equation 2.3-8 is used in Chapter 4 for calibrating the SF model. Equations 2.2-4 and 2.2-5 are used to provide the basic functional structure for the SF associated with all-land and all-sea water paths, respectively. For a mixed path, the SF is computed by using Millington's empirical method, Eqs. 2.2-1 through 2.2-3. Therefore, the task of model calibration is to obtain a mixed path TD calibration model which is consistent with available model calibration data so as to minimizes the difference between the measured and computed TDs.

3. CALIBRATION DATA ANALYSIS

3.1 CALIBRATION DATA

The U.S. Coast Guard-measured data provided to TASC for model calibration include TD data collected at land (all-land path) sites and at sea (part land and part sea water path) sites. The land data set includes three TDs/site: TD_w (TDW), TD_x (TDX) and TD_y (TDY), collected at 27 coastal sites distributed along the U.S. West Coast and shown (by triangles) in Fig. 3.1-1. The land site locations and TD measurements are as listed in Table 3.1-1. The sea data set consists of two TDs/site (TDX and TDY) collected at 23 sea sites located in the Southern California [between Point Arguello (near Santa Barbara) and San Diego] CCZ as shown (by circles) in Fig. 3.1-1. The sea data site locations and TD measurements are as listed in Table 3.1-2. Based on information from discussions with various sources and engineering judgement, the overall quality of the TD measurements including position reference errors is assumed to be between 0.1 - 0.2 μsec.

3.2 NONPARAMETRIC DATA ANLAYSIS

The purpose of nonparametric analysis of the calibration data is to identify

- Potential outliers that do not fit the data set
- Significant functional dependence(s) in the data on geophysical propagation parameters

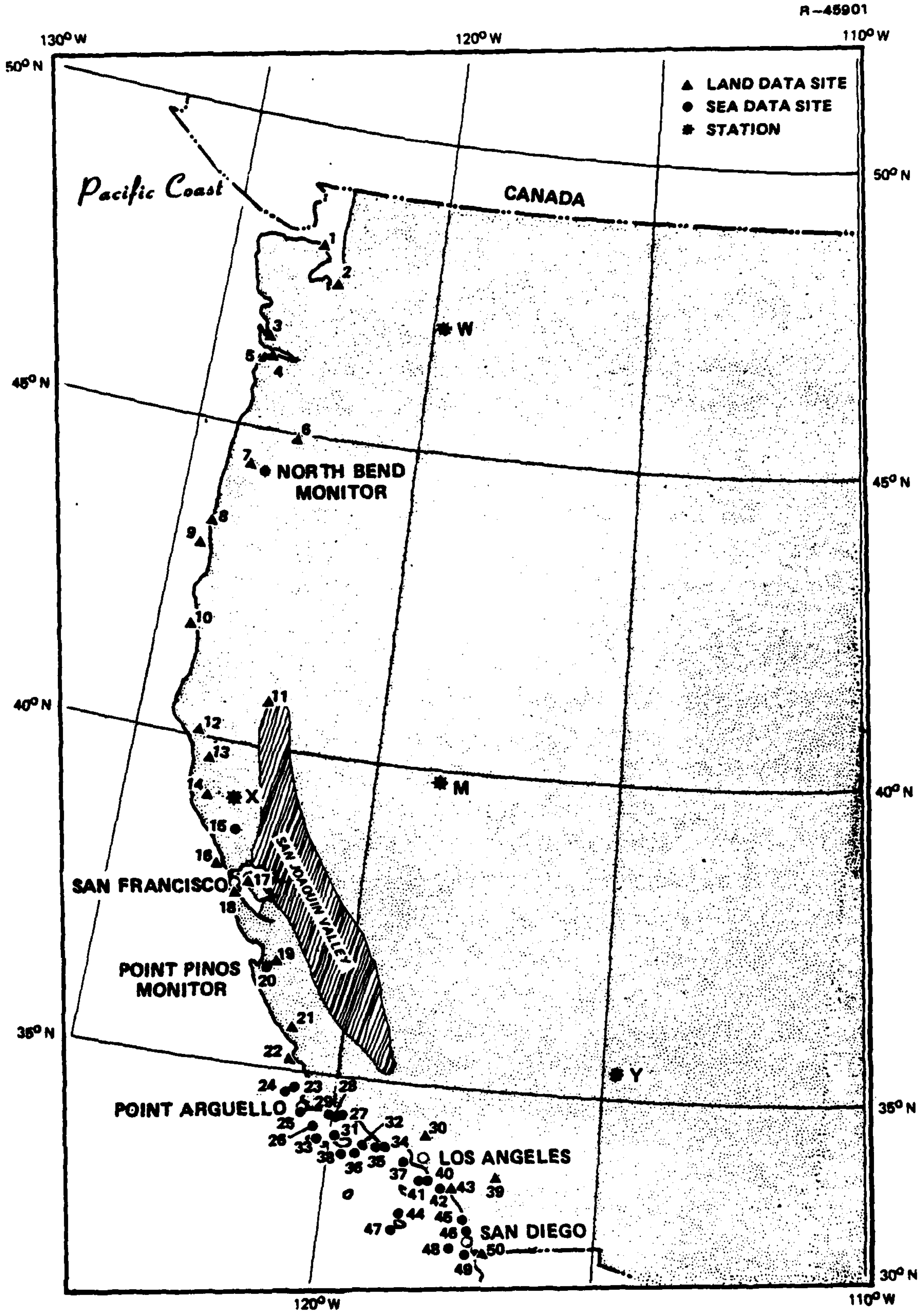

Figure 3.1-1 West Coast Loran-C Chain TD Measurement Data Site Locations

TABLE 3.1-1

LAND DATA SITE LOCATIONS AND TIME DIFFERENCE MEASUREMENTS

T-3549

SITE IDENTIFICATION		COORDINATES						TIME DIFFERENCE MEASUREMENTS		
		LATITUDE (NORTH)			LONGITUDE (WEST)			TDW	TDX	TDY
TASC	USCG	deg	min	sec	deg	min	sec	μsec	μsec	μsec
1	WORDEN	48	8	26.8	122	46	5.8	11297.483	28211.939	43850.462
2	PULLEY	47	27	2.2	122	22	58.3	11395.015	28228.481	*
3	TRAP CREEK	46	31	51.5	123	43	17.8	11919.090	28079.418	43907.798
4	MARITIME PIER	46	11	26.0	123	49	28.4	12075.060	28054.780	*
5	ASTOR	46	10	52.7	123	49	3.8	12078.347	28054.795	43915.396
6	HULT	44	57	46.4	122	42	49.2	12616.235	28114.235	43915.660
7	MARY 5	44	30	15.9	123	33	8.8	12913.894	27984.928	43933.169
8	NORTH BEND	43	24	36.2	124	14	27.9	13514.290	27801.218	43931.437
9	OLY	43	5	1.2	124	24	38.7	13679.803	27742.524	43923.179
10	MILLER	41	46	57.6	124	15	9.2	14353.579	27573.528	43872.846
11	BASS AZ SHIFTED	40	43	6.6	122	20	24.1	15164.430	27723.896	43859.591
12	PRATT SHIFTED	40	7	12.2	123	41	35.7	15179.554	27291.878	43725.263
13	DOS RIOS	39	42	26.2	123	17	46.4	15410.009	27225.781	43673.367
14	UKIAH AIRPORT	39	7	57.2	123	12	15.4	15618.499	27067.188	43560.515
15	X BASELINE EXT	38	46	57.0	122	29	44.5	*	26997.864	*
16	POINT REYES HILL	38	4	46.6	122	52	7.9	15946.970	27084.290	43290.030
17	TREASURE ISLAND	37	49	12.8	122	21	45.7	16091.059	27242.118	43199.210
18	POINT SAN MATEO	37	35	28.3	122	19	10.5	16133.682	27289.521	43121.187
19	SPENCE	36	35	43.4	121	32	48.0	16358.456	27596.470	42698.504
20	POINT PINOS (SAM)	36	37	55.0	121	56	5.6	16300.895	27493.970	42756.410
21	MT SENAS SHIFTED	35	52	57.3	120	49	20.1	16475.055	27795.923	42318.706
22	ISLAY	35	16	22.8	120	53	42.9	16483.635	27779.325	42118.129
27	PELICAN 2	34	24	18.0	119	50	39.9	16561.713	27967.883	41611.644
30	SISTER ELSIE SHIFTED	34	15	52.7	118	13	59.0	16595.832	28228.679	41116.852
39	RANGER SHIFTED	33	50	38.2	116	49	30.7	16570.525	28391.094	40593.120
43	DANA POINT	33	27	51.0	117	42	33.8	16592.861	28250.499	40612.136
50	SATELLITE	32	34	47.2	116	58	20.5	*	28288.773	40539.830

NOTE: Site Coordinates in WGS-72.
*No measurement data available.

TABLE 3.1-2
SEA DATA SITE LOCATIONS AND TIME DIFFERENCE MEASUREMENTS

T-3550

SITE IDENTIFICATION		COORDINATES						TIME DIFFERENCE MEASUREMENTS	
		LATITUDE (NORTH)			LONGITUDE (WEST)			TDX	TDY
TASC	USCG	deg	min	sec	deg	min	sec	μsec	μsec
23	2	34	43	55.2	120	44	36.9	27808.800	41916.000
24	1	34	42	57.5	120	47	5.1	27801.100	41920.000
25	7	34	26	38.2	120	9	15.8	27913.400	41698.300
26	3	34	26	18.9	120	35	11.7	27835.700	41796.300
28	9	34	23	3.0	119	47	32.8	27976.400	41592.400
29	6	34	18	1.2	120	19	32.6	27880.300	41659.000
31	5	34	11	39.1	119	49	14.1	27565.400	41548.000
32	4	34	5	57.0	119	23	1.4	28036.200	41410.500
33	8	34	5	9.2	120	12	48.8	27896.000	41615.700
34	13	34	2	52.0	119	0	14.9	28094.900	41294.500
35	12	34	0	48.3	119	11	41.8	28062.800	41339.100
36	11	33	57	3.7	119	33	9.7	28002.900	41419.400
37	14	33	55	11.1	118	30	15.0	28165.400	41122.500
38	10	33	55	6.5	119	42	23.6	27976.600	41450.900
40	15	33	41	44.9	118	21	29.9	28174.400	41036.000
41	16	33	40	44.5	118	10	48.0	28199.200	40981.300
42	17	33	32	5.9	117	47	31.3	28244.100	40846.100
44	19	33	6	50.7	117	21	48.1	28273.500	40675.300
45	18	33	3	23.4	118	31	15.0	28120.400	40975.600
46	20	32	55	28.7	117	17	4.5	28271.900	40638.200
47	21	32	51	4.4	118	37	45.6	28097.400	40974.300
48	23	32	37	46.8	117	13	18.0	28262.800	40601.000
49	22	32	37	38.8	117	31	27.4	28227.400	40674.000

NOTE: No TDW measurement data are available; site coordinates in WGS-72.

- Correlated trends between land and sea data
- Likely cause/effect relationship between data and geophysical characteristics.

For each TD component (i.e., TDW, TDX and TDY), the land and sea subsets were analyzed as a function of

- Range to secondary station
- Range to master station
- Differential range between secondary and master station
- Path bearing angle at master station
- Path bearing angle at secondary station.

Figures 3.2-1 through 3.2-3 present functional dependence plots of TDW, TDX and TDY components, respectively. Each figure shows adjusted TD measurements (Eq. 2.3-7) as a function of (a) site path bearing angle (from north) measured at the master station, (b) site path bearing angle (from north) measured at the secondary station, and (c) site differential range (differential primary phase delay) between secondary and master station, as defined in Fig. A.1-1 of Appendix A. (Note, the true value of an adjusted TD is simply the difference in SFs for the secondary and master station. Since sea data are not available for TDW, sea data plots are given for only TDX and TDY components.)

In addition to functional dependence trends, examinations of these figures reveals that there is a rather strong correlation between land and sea data subsets of each TD component. Figure 3.2-4 presents a composite plot of all three TD components for the ensemble of land and sea data as a function of differential range. This figure is presented to identify any common range-dependent trend (or trends) embodied in all of the three TD components.

Analysis of measurement data based on plots shown in Figs. 3.2-1 through 3.2-4, reveals the following:

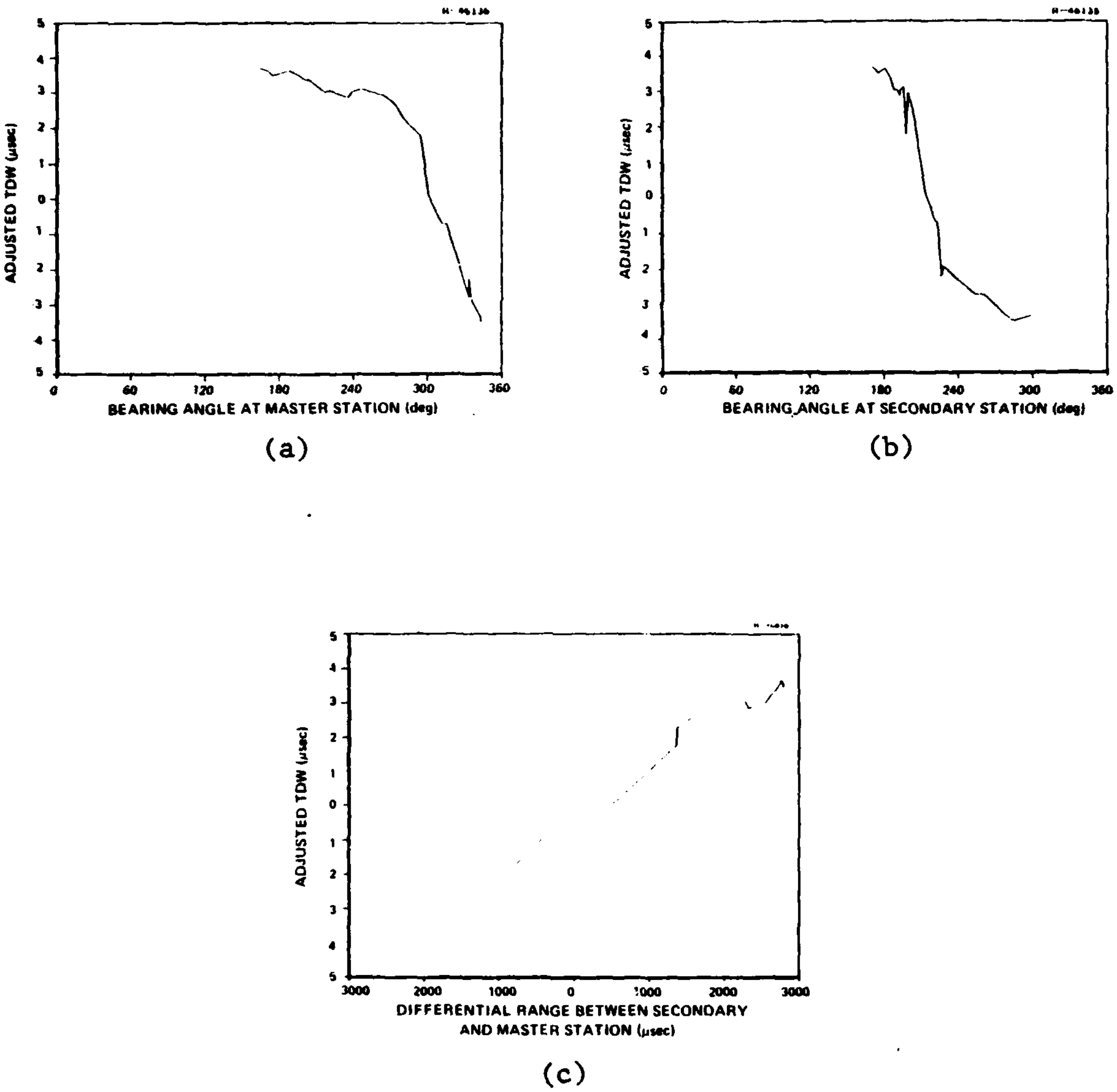

Figure 3.2-1 Adjusted TDW (Land Data) as a Function of (a) Path-Bearing Angle at Master Station (b) Path-Bearing Angle at W Secondary Station and (c) Site Differential Range Between W Secondary and Master Station

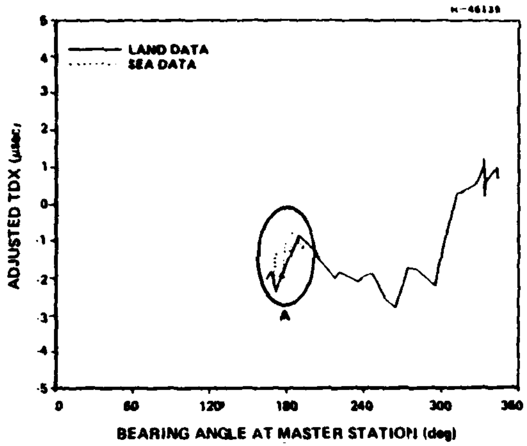

(a)

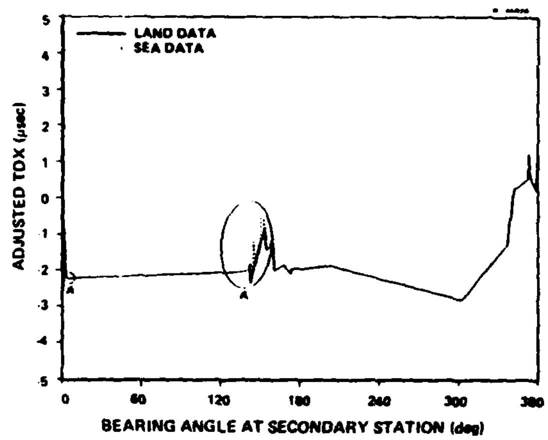

(b)

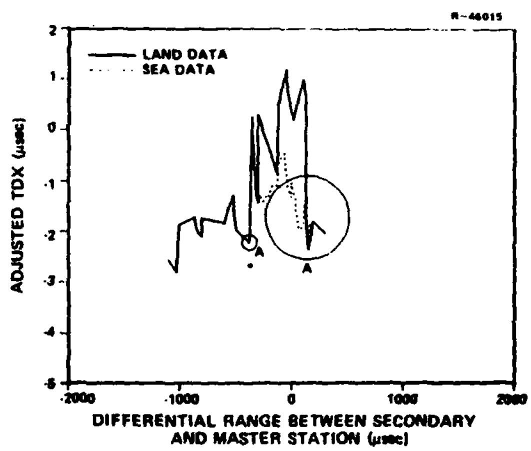

(c)

Figure 3.2-2 Adjusted TDX (Land and Sea Data) as a Function of (a) Path Bearing Angle at Master Station (b) Path Bearing Angle at X Secondary Station and (c) Site Differential Range Between X Secondary and Master Station

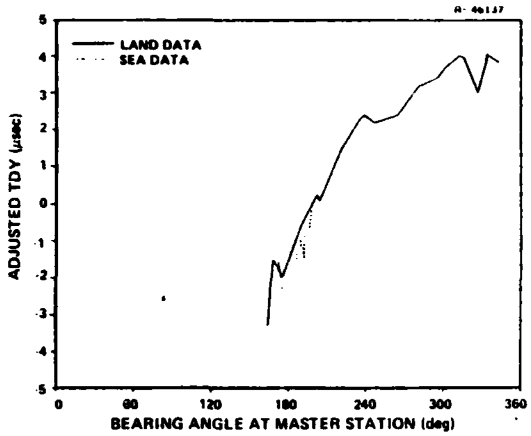

(a)

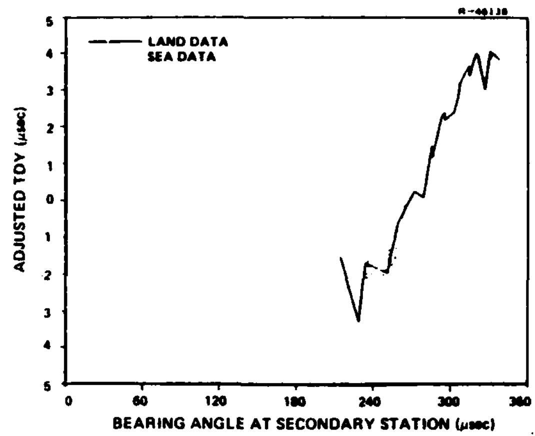

(b)

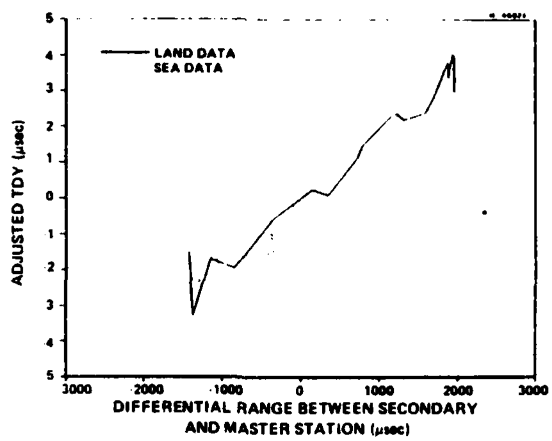

(c)

Figure 3.2-3 Adjusted TDY (Land and Sea Data) as a Function of (a) Path Bearing Angle at Master Station (b) Path Bearing Angle at Y Secondary Station and (c) Site Differential Range Between Y Secondary and Master Station

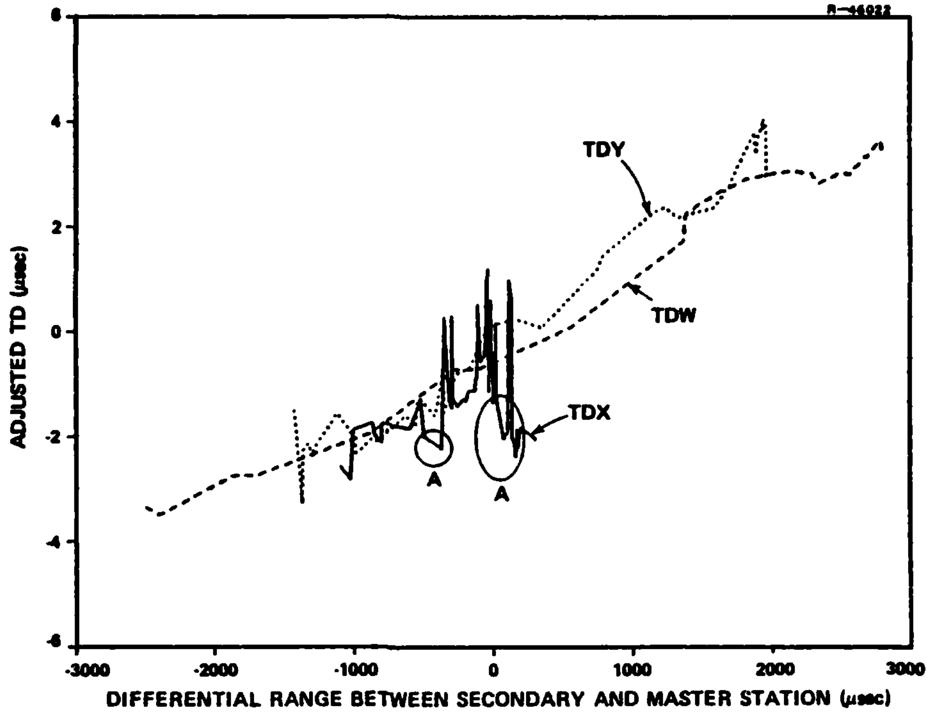

Figure 3.2-4 Adjusted TDW, TDX and TDY (both Land and Sea Data) Components As a Function of Site Differential Range Between Secondary and Master Station

- Dominant and very similar linear range-dependent trends in TDW and TDY but no identifiable trend in TDX
- Highly correlated trend between land and sea data as a function of both range and bearing angle
- TDX data behavior is significantly different than that of TDW or TDY; however, no obvious outliers in either TDW, TDX or TDY data
- TDX data identified as "A" are significantly different than the remainder of TDX data.

Further examination of TDX data (although not essential for the semi-empirical model development) indicated that all X station radial paths in the TDX data between bearing angles 3 and 150 deg from north (identified as "A" in Figs. 3.2-2 (c) and 3.2-4) exhibited behavior as a function of differential range grossly different than the remainder of TDX data. This suggested the possibility that a terrain with propagation properties different from those of the remaining chain coverage area may exist in the region within these bearing angles. Indeed, the location of the San Joaquin Valley (see Fig. 3.1-1) whose conductivity is higher than that of the surrounding area by an order of magnitude (Ref. 10), is roughly defined by this region. Because of the San Joaquin Valley's orientation relative to the X station and the shoreline, all X station radial paths leading to the CCZ between Los Angeles and San Diego will be significantly impacted by the presence of the valley and will exhibit signal propagation behavior drastically different than the rest of the X station signal coverage area. Note that the TDW and TDY data recorded along the coastline are not expected to be significantly affected by the high conductivity of the valley. This is because the propagation path segment through the valley is a small percentage of the total propagation path for the M, W, and Y stations.

3.3 SUMMARY

Table 3.3-1 presents a summary of the data available for calibrating the West Coast TD grid model. Land data are distributed along the West Coast from Canada to San Diego while the sea data are concentrated between Point Arguello and San Diego. The overall quality of the calibration data is not known, but assumed to have an rms accuracy of 0.1 -0.2 μsec.

TABLE 3.3-1

WEST COAST MODEL CALIBRATION DATA BASE SUMMARY

TYPE OF DATA	NUMBER OF DATA SITES	NUMBER OF MEASUREMENTS			TOTAL NUMBER OF TD DATA POINTS
		TDW	TDX	TDY	
Land	27	25	27	24	76
Sea	23	*	23	23	46
Combined Land and Sea	50	25	50	47	122

*No data available.

The data are considered to be consistent with the expected theoretical behavior. The "apparently anomalous" behavior in TDX data seem to have been caused by the San Joaquin valley region whose conductivity is an order of magnitude higher than the surrounding region.

The land and sea TD data exhibit similar characteristics as a function of both station range and bearing angle at the station. These similar characteristics are caused by common overland path segments (i.e., conductivity) in land and sea data, and suggest that there is a uniform land/sea water interface vs bearing angle effect in the sea data, which covers a narrow range of bearing angles. Additional data covering a wider range of bearing angles are required to validate the observed uniformity in the interface effect. The observed data characteristics suggest the use of both range and bearing angle dependences in the TD model structure. Furthermore, especially over the West Coast CCZ sea data collection region, these characteristics indicate that land data alone may be sufficient to calibrate a mixed path model.

4. CALIBRATED TD MODEL

4.1 INTRODUCTION

The purpose of this chapter is to present an accurate TD grid calibration algorithm for the West Coast Loran-C chain CCZ. Two alternative model calibration approaches, shown as A and B in Fig. 4.1-1, are considered. Approach A is designed to assess the utility of using only land based data for CCZ model calibration as compared to using both land and sea based data in approach B. In approach A, the land model is calibrated while the sea model is based on theory (i.e., with *a priori* known coefficients); in approach B, the composite land and sea model is calibrated with the combined land and sea data. Both approaches apply Millington's empirical method to combine land and sea SFs to obtain a mixed path SF. The model calibration procedure for both approaches is detailed in the next section.

4.2 TD MODEL CALIBRATION EQUATIONS

4.2.1 Adjusted TD Measurement Equation

It is convenient to model the transformed form of the TD measurements, i.e., adjusted TD measurements, given by Eq. 2.3-8 and repeated below:

$$ATD_i \equiv z_i = (SF_i - SF_m) + v_i \qquad (4.2\text{-}1)$$

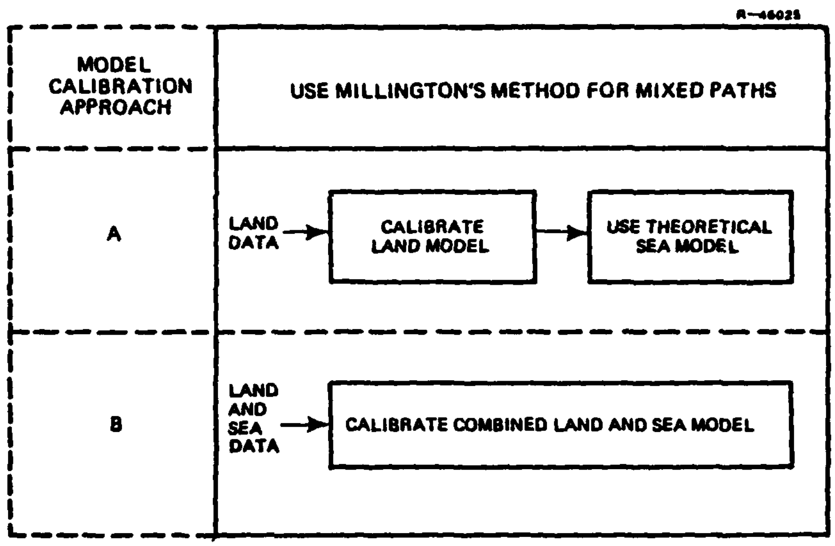

Figure 4.1-1 Alternative Model Calibration Approaches

where SF_i (and SF_m) are the SFs associated with the signal paths from i^{th} (= w, x or y) secondary (and master) stations and v_i is the total measurement error associated with TD_i.

4.2.2 Sea SF Model

The structure considered for the sea SF model is

$$SF = \begin{cases} \dfrac{a_{-1}}{T} + a_o + a_1 T \ \mu sec, & \text{if } 10 \le T \le 540 \ \mu sec \\ \dfrac{a_{-1}'}{T} + a_o' + a_1' T \ \mu sec, & \text{if } T > 540 \ \mu sec \end{cases} \qquad (4.2\text{-}2)$$

where T is the primary phase delay (or range); a_k and a_k' (k = -1, 0 and 1) are sea coefficients considered as known (no uncertainty) for approach A and unknown (uncertain) for approach B. The sea model coefficient values for approach A are (Ref. 9)

$$a_{-1} = 2.741$$
$$a_o = -0.0114$$
$$a_1 = 0.0003277 \qquad (4.2\text{-}3)$$
$$a'_{-1} = 129.043$$
$$a'_o = -0.408$$
$$a'_1 = 0.0006458$$

4.2.3 Land SF Model

A general polynomial model structure for the land SF associated with a station is given by Eq. 2.2-4. By specializing this model structure to the West Coast chain CCZ service area and chain topography, and incorporating the results of calibration data analysis, the following two candidate forms for the land SF model were considered:

- "Localized" Range/Bearing (LRB) Model

$$SF_j = A_o + [A_1 + B_1 \ f_x(\beta_x)] \ T_j \ \mu\text{sec} \qquad (4.2\text{-}4)$$

- "Generalized" Range/Bearing (GRB) Model

$$SF_j = A_o + A_1 \ T_j + \sum_{\ell=1}^{L} [C_{j\ell} \sin \ell\beta_j + D_{j\ell} \cos \ell\beta_j] \ \mu\text{sec} \qquad (4.2\text{-}5)$$

where A_o, A_1, B_1, $C_{j\ell}$ and $D_{j\ell}$ are uncertain model coefficients, β_j is the path bearing angle at the j^{th} (= w, x, y or m) station and T_j is the path range to the j^{th} station; function $f_x(\beta_x)$ is zero for all chain stations except for the X station.

For the X station, f_x is zero unless the X station radial (signal path) passes through the San Joaquin Valley, then it is unity.

The LRB model is purposely kept as simple (fewest uncertain model coefficients) as possible yet designed to embody distortions (warpages) to the X station SF caused by the San Joaquin valley. The GRB model, on the other hand, includes bearing angle dependences for all four chain stations instead of the X station alone, as is the case in the LRB model. Consequently, the GRB model is relatively more complex and is expected to exhibit performance superior to the LRB model. Note that a calibrated model is expected to be accurate and applicable only over the extent of ranges and bearing angles embodied in the calibration data. Hence, outside the region covered by the calibration data, the model may not be as accurate as within the data coverage region.

4.2.4 Mixed Path SF Computations

The SF over a mixed path is computed using Millington's empirical equations, Eqs. 2.2-1 through 2.2-3. In these equations, all terms except $SF(\sigma_L, T_S)$ in Eq. 2.2-3 can be computed with land and sea SF models described in Sections 4.2.2 and 4.2.3. The $SF(\sigma_L, T_S)$ is the SF of a fictitious land path of length T_S (the sea segment of the actual mixed path) which is usually much smaller than any of the actual land segment path lengths embodied in the West Coast land calibration data base. Consequently, the land SF model to be developed with the calibration data base cannot be used to compute the term $SF(\sigma_L, T_S)$ in Eq. 2.2-3. Therefore, the following theoretical polynomial land SF model is used:

$$SF(\sigma_L, T_S) = \frac{0.795}{T_S} + 0.439 + 0.00245\, T_S \quad \mu\text{sec} \qquad (4.2\text{-}6)$$

where T_S is in μsec. This polynomial model was derived by fitting it to the homogeneous/smooth earth theoretical predictions (Ref. 4). The coefficients of this model correspond to an average ground conductivity of 0.003 mhos/m, which is the estimated average conductivity of the West Coast chain coverage area based on the nonparametric data analysis results (Chapter 3) and homogeneous/smooth earth theory (Ref. 4). Mixed path SFs derived from the combination of land and sea SF models, as per Eqs. 2.2-1 through 2.2-3, are then incorporated in the adjusted TD measurement equation, Eq. 4.2-1, which is calibrated with the measurement data as described in the next section.

4.3 MODEL CALIBRATION

4.3.1 Calibration Procedure

An overview of the West Coast TD grid calibration procedure is illustrated in Fig. 4.3-1. The first step in the model calibration procedure is to hypothesize candidate model structures for the land and sea SF models. In approach A, the sea model is known (theoretical) and therefore only the land model is hypothesized as opposed to approach B where both land and sea models are postulated.

Next, mixed path SFs are substituted to form adjusted TD measurements (Eq. 4.2-1) which can be symbolically written in matrix form (Ref. 3) as

$$\underline{z} = H\,\underline{x} + \underline{v} \qquad (4.3\text{-}1)$$

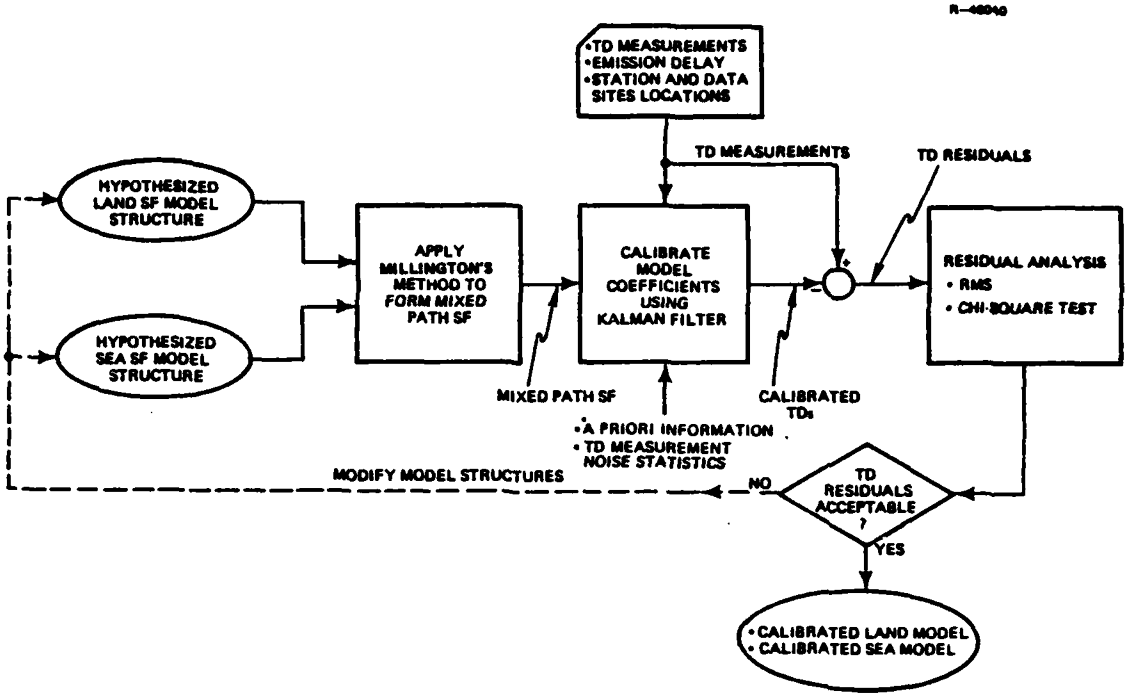

Figure 4.3-1 TD Grid Calibration Procedure

where the measurement vector is

$$\underline{z} = \begin{bmatrix} ATD_w \\ ATD_x \\ ATD_y \end{bmatrix} \tag{4.3-2}$$

The observation matrix, H, is a function of range and bearing angle of station paths associated with the TD. The state vector, $\underline{x}$, is a vector of uncertain model coefficients which are to be estimated from data. The TD measurement error vector is $\underline{v}$ given by

$$\underline{v} = \begin{bmatrix} v_w \\ v_x \\ v_y \end{bmatrix} \tag{4.3-3}$$

where TD component (i.e., TDW, TDX or TDY), and hence ATD component, measurement errors are assumed to be random with zero mean.

The next step in the calibration procedure is to provide a priori information on the initial estimates and uncertainties of model coefficients, and TD measurement error statistics to the coefficient estimation algorithm. The Kalman filter (Ref. 3) provides a convenient method to estimate the state vector (coefficients) with a zero mean using the adjusted TD measurements. The a priori information was developed by a combination of data anlaysis results and expected theoretical behavior of Loran-C signals over land and sea water paths. In particular, the sea water SF model coefficients were constrained to reasonable theoretical limits to warrant the calibrated model useful beyond the CCZ region (where no data were available for model calibration).

Initial attempts to calibrate candidate West Coast TD models consistently yielded TD residuals with an rms level of about 0.4 μsec. Therefore, TD component measurement error in the calibration procedure was assumed to be 0.4 μsec. Note, 0.4 μsec error includes receiver measurement error of 0.1 - 0.2 μsec (Chapter 3), data site position location reference errors, unmodeled TD warpage conditions and emission delay variations from site-to-site.

More than 20 candidate GRB model structures (Eq. 4.2-5) with varying numbers of harmonic terms as well as the single LRB model structure (Eq. 4.2-4) were considered for the land SF model. The sea SF model was always chosen to be 3-term, range-dependent model given by Eq. 4.2-2.

Each candidate land SF model in combination with the theoretical sea SF model (approach A), or semi-empirical sea SF

model (approach B), was calibrated with land data (approach A) or combined land and sea data (approach B). For each candidate combination, an associated candidate observation matrix and a state vector were developed.

Performance of each calibrated candidate combined land and sea model was evaluated in terms of the statistical reasonableness of the calibrated model fit to the data. Statisitacal reasonableness was quantified as indicated in Fig. 4.3-2 in terms of the standard deviation of individual TD component site residuals and the chi-square test which evaluates the fit of the three- (or two-) dimensional TD site residual (i.e., all TD components together at a site) to the data.

4.3.2 Calibrated Models

Of the candidate GRB land SF models considered, the TD model with the following GRB functional form yielded the best performance:

$$SF_j = A_o + A_1 T_j + \sum_{\ell=1}^{2} [C_{j\ell} \sin \ell\beta_j + D_{j\ell} \cos \ell\beta_j] \tag{4.3-4}$$

where

j = w, x, y or m station

$C_{w1} = C_{x1} = C_{y1} = 0$

$D_{w1} = D_{x1} = D_{y1} = 0$

$C_{x2} = 0$

$D_{y2} = 0$

Table 4.3-1 describes the number of uncertain coefficients included in the "best" GRB model and the LRB model under each of the two calibration approaches considered.

TABLE 4.3-1

NUMBER OF COEFFICIENTS IN LRB AND GRB TD MODELS

T-3593

APPROACH	LOCALIZED RANGE/BEARING (LRB) MODEL					TOTAL NUMBER OF COEFFICIENTS	GENERALIZED RANGE/BEARING (GRB) MODEL					TOTAL NUMBER OF COEFFICIENTS
	RANGE (T)		BEARING β	BIAS			RANGE (T)		BEARING β	BIAS		
	LAND	SEA	LAND	LAND*	SEA†		LAND	SEA	LAND	LAND*	SEA†	
A CALIBRATED LAND MODEL (THEORETICAL SEA MODEL)	1	–	1	3	–	5	1	–	8	3	–	12
B CALIBRATED COMPOSITE LAND AND SEA MODEL	1	4	1	3	2	11	1	4	8	3	2	18

*TDW, TDX AND TDY.
†TDX AND TDY.

Note, in approach A where only land data are used to calibrate the land model, one bias state (coefficient) per land TD component is required in the TD model (see Table 4.3-1) to account for a possible constant bias (shift) in the secondary station emission delay and the unobservable biases in the land SF models. However, in approach B where both land and sea data are used to calibrate the composite land and sea model, an additional bias state per sea TD component is included as shown in Table 4.3-1) to result in zero-mean residuals. If sea TD bias states are not included in the model, the mean TD residual is non-zero, and furthermore the rms TD residual is significantly larger than that obtained with sea TD bias states. Thus, a total of three land TD bias states (for TDW, TDX and TDY) are included in the TD model calibrated in approach A, while three land and two sea TD bias states (for TDX and TDY) are used in the TD model calibrated in approach B. As expected, the magnitude of the sea bias states in the model calibrated in approach B were roughly the same as the corresponding means in the sea TD residuals obtained in approach A where sea TDs are computed using a calibrated land model and the theoretical sea model, Eqs. 4.2-2 and 4.2-3. There is not sufficient data to identify the likely sources of the observed sea TD biases. The land/sea water interface "phase recovery" effect (Ref. 7) may be responsible for part of the observed sea TD biases.

4.4 CALIBRATED MODEL PERFORMANCE

4.4.1 Calibration Data Base

Table 4.4-1 summarizes the rms TD residuals for the LRB and GRB TD models calibrated with (1) land data alone (approach A) and (2) combined land and sea data (approach B). In this table, the rms value of the residuals at the 46 sea

TABLE 4.4-1

PERFORMANCE COMPARISON OF LRB AND GRB MODELS

T-3566

CALIBRATION APPROACH	MODEL	NUMBER OF CALIBRATION DATA POINTS			RMS TD RESIDUAL - μSEC	
		LAND	SEA	TOTAL	OVER SEA DATA POINTS (46)	OVER COMBINED LAND AND SEA DATA POINTS (122)
A Calibrated Land Model (Theoretical Sea Model)	LRB	76	-	76	0.703	0.636
	GRB	76	-	76	0.769	0.570
B Calibrated Composite Land and Sea Model	LRB	76	46	122	0.343	0.521
	GRB	76	46	122	0.350	0.390

calibration TD data points (and also for over the entire set of 122 land and sea calibration TD data points) are presented.

Comparison of sea residual statistics (Table 4.4-1) obtained with the LRB and GRB models shows similar performance for both models in either approach. However, calibration approach B yields a factor of two improvement in the sea rms residual over those obtained in approach A. Thus, from considerations of sea residuals alone, approach B is preferred over approach A. Further comparison of rms residuals obtained with the LRB and GRB models (Table 4.4-1) over the entire set of land and sea calibration data points indicates that the GRB model yields superior performance. Therefore the GRB model calibrated with land and sea data was selected as the "best" performance TD model for calibrating the West Coast Loran-C chain. The residual statistics obtained with the GRB model for the indicated TD components and data sets are summarized

in Table 4.4-2. The details of the calibrated GRB model and LRB model algorithms are given in Appendix A.

TABLE 4.4-2
TD RESIDUAL STATISTICS OF GRB MODEL
OVER CALIBRATION DATA BASE (APPROACH B)

CALIBRATION DATA BASE	RMS TD RESIDUAL - μsec			
	TDW	TDX	TDY	COMBINED TD COMPONENTS
Land	0.308	0.501	0.382	0.408
Sea	*	0.388	0.306	0.350
Combined Land and Sea	0.308	0.457	0.347	0.390

*No calibration sea data available.

Figure 4.4-1 presents the TD residuals (solid curve) at each land and sea data site obtained with the calibrated West Coast GRB model. The data collection sites are arranged in order from north to south. For comparison, Fig. 4.4-1 also shows the calibration data (dotted line) and the adjusted TD measurements. Both data and residuals have breaks (or gaps) at sites where no measurement data are available. (Note, there are no sea data for the TDW component.)

4.4.2 Validation Data Base

The calibrated model was also evaluated at the 25 sea sites listed in Table 4.4-3, the coordinates of which were specified by the U.S. Coast Guard. The computed TDs at the validation sites, as listed in Table 4.4-3, were forwarded to the U.S. Coast Guard for comparison with TD measurements. The rms TD residual over the ensemble of all TDs (i.e., 25-TDX and 25-TDY) computed by the U.S. Coast Guard is 0.42 μsec, a

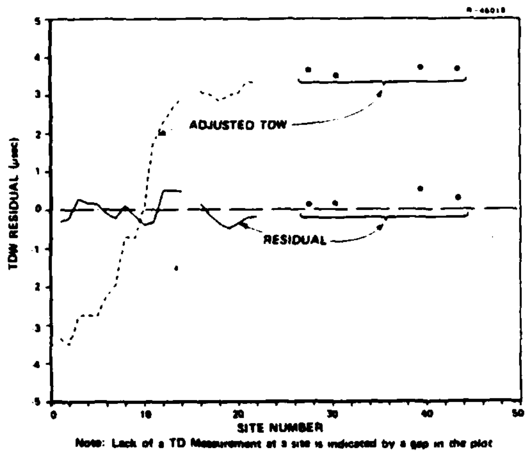

(a) TDW Residual

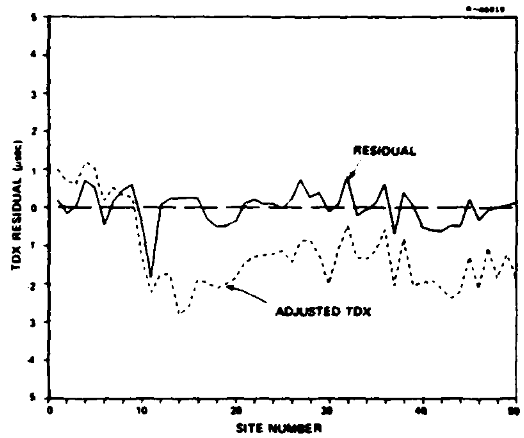

(b) TDX Residual

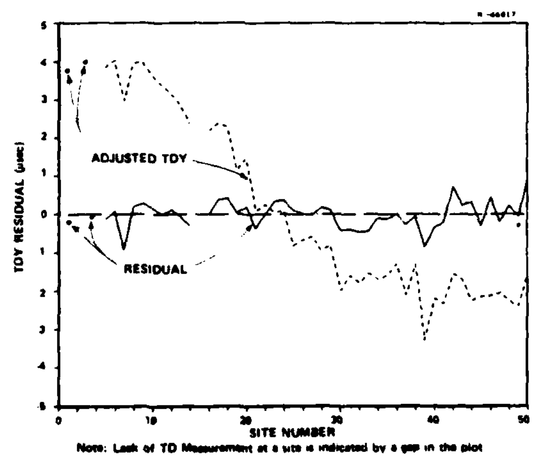

(c) TDY Residual

Figure 4.4-1 TD Residuals for GRB Model Calibrated with Combined Land and Sea Data (Approach B)

TABLE 4.4-3

VALIDATION DATA S E LOCATIONS AND COMPUTED TIME DIFFERENCES

SITE IDENTIFICATION		SITE COORDINATES						STATION-TO-SITE PATH SEGMENT LENGTH - km						COMPUTED TIME DIFFERENCE -μsec	
		LATITUDE (NORTH)			LONGITUDE (WEST)			MASTER		X SECONDARY		Y SECONDARY			
TASC	USCG	deg	min	sec	deg	min	sec	LAND	SEA	LAND	SEA	LAND	SEA	TDX	TDY
55	A	34	34	18.3	120	39	40.3	540.730	35.548	369.248	126.096	525.659	15.832	27823.045	41850.751
56	B	34	22	55.9	120	29	26.2	573.809	18.769	379.915	140.449	484.519	45.898	27851.545	41759.037
57	C	34	14	45.3	120	3	51.6	573.227	25.936	517.352	31.280	441.858	54.201	27924.840	41622.215
58	D	34	24	20.2	119	57	42.6	574.267	5.815	527.953	8.180	473.552	8.935	27946.775	41640.688
59	E	34	4	40.1	120	2	33.2	574.106	43.083	514.429	52.215	423.325	76.097	27924.777	41573.234
60	F	34	6	0.0	119	51	26.5	575.859	32.221	524.103	46.930	420.578	61.405	27956.404	41533.364
61	G	34	23	15.7	119	36	56.1	574.088	3.430	547.187	4.530	446.169	5.907	28007.257	41547.591
62	H	34	8	3.5	119	35	29.7	575.296	29.913	546.776	31.097	419.793	38.079	28002.174	41474.503
63	I	34	4	3.2	119	32	18.9	577.552	34.476	546.525	40.150	418.031	37.567	28008.621	41444.022
64	J	34	6	42.3	119	11	50.9	592.024	12.768	573.137	23.665	413.075	11.191	28066.577	41363.627
65	K	33	48	45.1	118	45	45.3	612.293	24.854	606.876	38.620	361.382	38.626	28121.013	41174.40[illegible]
66	L	33	39	41.7	118	22	5.7	621.233	33.947	627.728	50.977	360.704	14.533	28171.597	41032.912
67	M	33	22	6.4	119	5	51.2	601.195	85.605	545.988	128.332	364.659	85.926	28051.470	41177.679
68	N	33	28	41.1	119	25	32.3	584.152	92.161	530.477	119.862	359.571	112.054	28006.582	41282.933
69	O	33	44	50.7	120	4	12.6	574.537	79.227	505.465	54.391	403.107	110.929	27913.541	41459.930
70	P	33	52	5.8	119	58	51.6	576.267	62.944	513.080	77.255	412.386	69.171	27930.315	41506.854
71	Q	33	53	53.9	119	50	39.7	583.248	53.819	519.360	72.700	411.378	77.162	27953.187	41480.545
72	R	33	19	43.9	118	3	45.5	650.583	43.629	627.957	97.117	332.617	39.983	28195.823	40892.276
73	S	33	21	7.1	117	36	36.2	682.331	14.537	709.726	36.445	330.200	8.077	28257.403	40768.703
74	T	33	15	0.4	118	10	34.3	648.823	53.162	632.112	94.855	332.551	53.753	28176.298	40912.091
75	U	32	50	35.5	118	19	27.0	619.746	126.314	576.567	182.680	330.042	95.592	28137.518	40856.448
76	V	32	52	42.4	118	1	4.4	650.541	93.814	614.137	155.826	330.812	70.966	28178.260	40622.360
77	W	32	47	5.6	118	32	40.3	608.917	142.534	554.349	200.869	330.443	114.977	28106.122	40744.559
78	X	32	41	55.5	118	1	37.9	650.313	113.811	604.960	181.828	331.313	85.010	28169.034	40804.941
79	Y	32	39	50.2	117	46	45.6	657.805	112.586	624.135	177.693	331.124	72.000	28198.281	40739.931

factor of four improvement over the original U.S. Coast Guard TD grid charting procedures (Ref. 10). Note, the rms residual over the validation data points (0.42 μsec) is approximately the same value as that obtained over the calibration data points (0.35 μsec).

4.5 SUMMARY

Land data alone (approach A) can be used to calibrate the West Coast CCZ grid to an rms accuracy of approximately 0.8 μsec. Use of sea data in addition to land data (approach B) provides a factor of two improvement in the CCZ grid accuracy. The GRB model calibrated with combined land and sea data yields the best overall rms TD residual performance and was therefore selected as the West Coast calibrated TD grid model. The calibrated GRB model has an rms TD error of 0.35 μsec over sea calibration data points which would result in an rms position error of 340 m in the West Coast CCZ if TDX and TDY LOPs are utilized for the position fix by a user with a "perfect" receiver. The rms TD error of the calibrated model over the U.S. Coast Guard sea validation data points (not used in model calibration) is 0.42 μsec resulting in a factor of four improvement over the original charting procedures. This demonstrates that semi-empirical grid calibration techniques are effective for calibrating an accurate Loran-C grid for the Coastal Confluence Zone.

5. MODEL ACCURACY SENSITIVITY ANALYSIS

5.1 INTRODUCTION

The sensitivity analysis presented herein assesses the operational practicality of adopting semi-empirical techniques (or models) as a TD grid calibration tool for Loran-C chain CCZ regions. Key operational issues are the quantity and distribution of grid calibration data required to achieve a desired grid accuracy. This section examines the accuracy of the West Coast semi-empirical GRB TD model grid (developed in Chapter 4) in terms of the quantity and distribution of data used for calibrating the model. Based on West Coast sensitivity analysis results, calibration data collection guidelines are formulated to aid in the design of future semi-empirical grid calibration efforts.

5.2 ANALYSIS

5.2.1 Sensitivity and Evaluation Data Bases

Two mutually exclusive data bases (Table 5.2-1) are formed, for the sensitivity analysis studies, out of the available TD measurement data used in Chapter 4 to calibrate the West Coast TD grid model. The two data bases are refered to as the sensitivity data base and the evaluation data base. The sensitivity data base consists of both land and sea data sites (distributed from Canada to San Diego), subsets of which are used to calibrate the sensitivity analysis model. The accuracy of each calibrated model is assessed with the

TABLE 5.2-1

SENSITIVITY AND EVALUATION DATA BASES SUMMARY

DATA BASE	NUMBER OF DATA SITES			NUMBER OF TD DATA POINTS		
	LAND	SEA	TOTAL	LAND	SEA	TOTAL
Sensitivity	27	12	39	76	24	100
Evaluation	-	11	11	-	22	22
Combined	27	23	50	76	46	122

evaluation data base which includes only sea sites distributed in the Southern California CCZ (between Point Arguello and San Diego).

5.2.2 Approach

A number of subsets of the sensitivity data base are used to calibrate the sensitivity model. These subsets included

- Uniform distributions of combined land and sea calibration data sites as shown in Fig. 5.2-1
- Clusters of land calibration sites (located either north or south of San Francisco) with uniform distribution of sea sites located in Southern California, as shown in Fig. 5.2-2.

Each of the calibration data sets (subsets of the sensitivity data base) are used (one at a time) to calibrate the sensitivity model by the calibration procedure described in Section 4. The calibrated model is then used to compute the TDs and resulting TD residuals at <u>all</u> sites in the combined

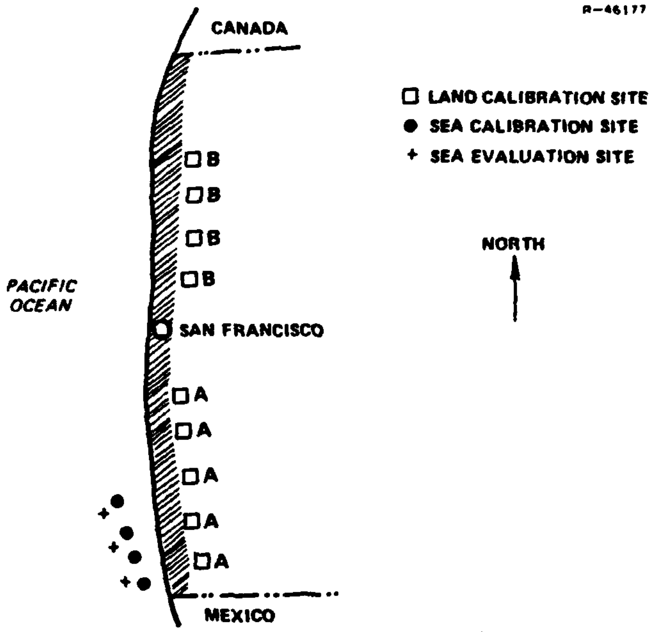

Figure 5.2-1 Illustration of Clustered Land Calibration Sites and Uniformly Spaced Sea Calibration Sites

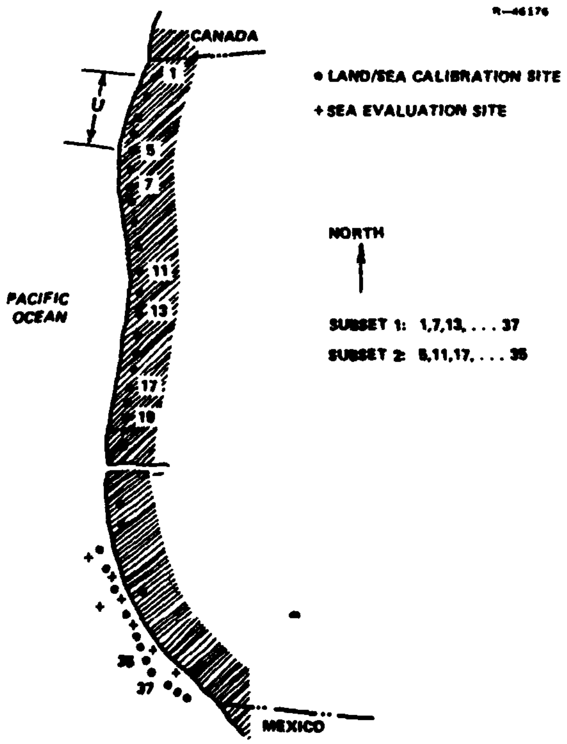

Figure 5.2-2 Illustration of Uniformly Distributed Combined Land and Sea Calibration Data Sites

data base. The rms of the TD residuals of each calibrated model is then computed over (1) the "evaluation sites" (i.e., ensemble of all TD components at all sites in the evaluation data base) and (2) "all sites" (i.e., ensemble of all TD components at all sites in the combined data base).

5.2.3 Sensitivity Analysis Results

The rms TD residuals obtained with the GRB TD model calibrated with subsets of the sensitivity data base are shown in Fig. 5.2-3 as a function of quantity and distribution of the calibration data, where

- The quantity of calibration data is expressed as a percentage of TD data points in the combined data base (which includes data points in both sensitivity and evaluation data bases)
- The data distribution is keyed as a bar (representing uniform data site distribution) or a triangle (denoting clusters of calibration data sites)
- The length of a bar shows the spread of the computed rms TD residuals obtained for models calibrated with several uniformly distributed subsets of the sensitivity data base, each containing approximately the same number of data points
- Adjacent solid and open areas, bars or triangles, are the corresponding rms TD residuals over all sites and evaluation sites, respectively.

The rms residuals shown for 100 percent of the data are the residuals of the model calibrated with all the available data in Chapter 4 (i.e., including evaluation data) and are shown for comparison purposes. Brief explanations of the observed calibrated model accuracy behavior for both clustered and

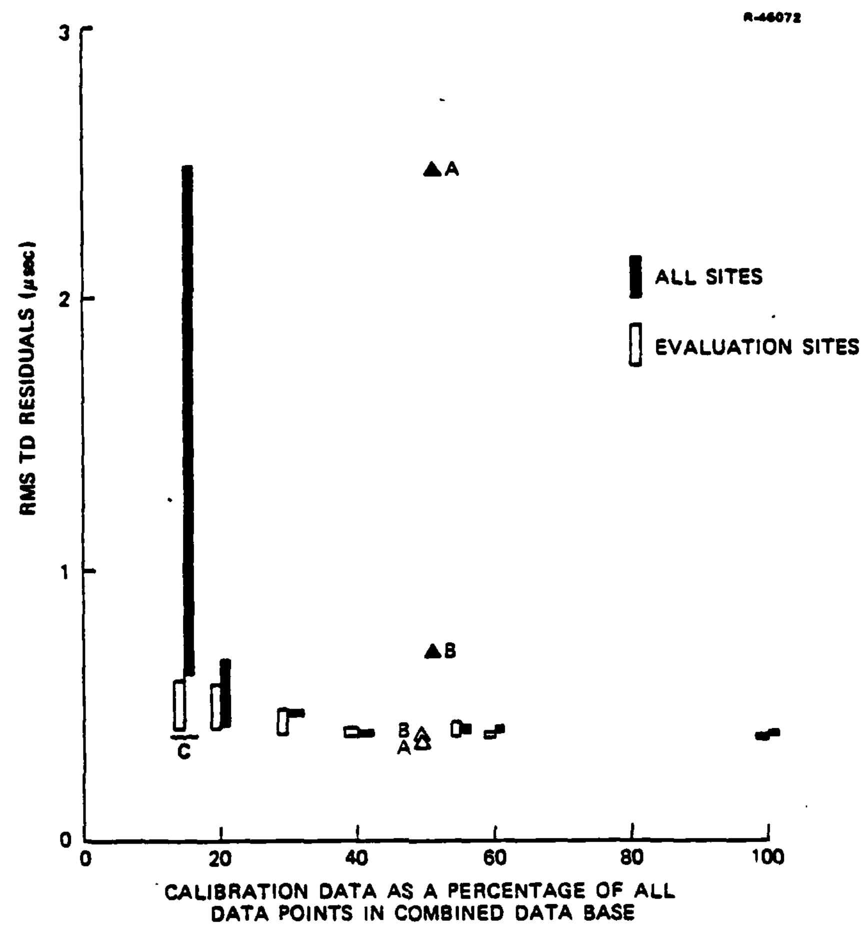

Figure 5.2-3 Model Accuracy Sensitivity to Quantity and Distribution of Calibration Data

uniformly distributed calibration data conditions are presented in the following sections.

5.2.4 Clustered Sets of Calibration Data

Two specific examples of clustered data sets are shown in Fig. 5.2-3. Calibration data set A (see Fig. 5.2-1) includes all land data south of San Francisco and all sea data available in the sensitivity data base (also south of San Francisco). No calibration data north of San Francisco is contained in data set A. Consequently, the model calibrated with data set

A performs poorly over data sites north of San Francisco as manifested by the high rms residual computed over all sites. On the other hand, the calibrated model is expected to exhibit excellent performance in the region south of San Francisco where all of the evaluation sites are located. This performance is manifested by the low residual value computed over the evaluation sites.

Calibration data set B includes land data north of San Francisco and all sea data (south of San Francisco) -- thus, the sensitivity data base includes data distributed (although not uniformly) over the entire West Coast. Consequently, the model calibrated with data set B is expected to have a relatively better residual performance, especially over the data sites located north of San Francisco, than the model calibrated with A. This is manifested in Fig. 5.2-3 by a smaller rms residual over all sites for case B. Note, evaluation site residuals for both cases are comparable, since both subsets A and B include calibration data over the region covered by the evaluation sites. From the comparison of calibrated model performance for the two sets, it is concluded that the calibration data set must be representative of the region to be calibrated.

5.2.5 Uniformly Distributed Calibration Data Sets

A number of uniformly distributed calibration data sets with varying data density were analyzed. As an example, consider the computed spread of residuals, labeled as C in Fig. 5.2-3. Adjoining residual bars labeled all sites and evaluation sites correspond to the use of 18 calibration data points, roughly 13 percent of the combined data. These bars ("C") depict the spread of computed rms residuals for four different uniformly distributed calibration data subsets formed

from the sensitivity data base by retaining every sixth data site. For this case, two of the four subsets of the sensitivity data base considered are labeled 1 and 2 in Fig. 5.2-1. Subsets 1 and 2 are similar except subset 2 does not span the northern tip of the U.S. West Coast area (identified as "U" in Fig. 5.2-2) and covered by sites 1 through 4. Thus, the model calibrated with subset 2 extrapolates over "U" while the model calibrated with subset 1 interpolates over "U". Therefore, the all site residual performance of the model calibrated with subset 2 is inferior to the performance using subset 1, as manifested by the highest all site residual value. There is very little spread, as expected, in the evaluation site residuals because all four calibration data subsets cover the region of evaluation sites.

As expected, the spread in rms residual values (Fig. 5.2-3) associated with both all sites and with the evaluation sites decreases with increasing density of the data in a uniformly distributed calibration data set. <u>No significant improvement in the West Coast calibrated grid rms residual performance is observed with the use of more than 40 percent of the available data for model calibration data</u>.

5.3 SUMMARY

Based on the West Coast model accuracy sensitivity analysis results, it is concluded that

- A uniform distribution of 50 percent of the available measurement data provides a CCZ TD grid with an rms accuracy of 0.4 μsec as compared to 0.35 μsec with 100 percent of data

- Data collection sites should be selected to provide a relatively uniform distribution along the coast with an average spacing of 100-200 km over the region of interest (as compared to 50-100 km for land sites and ~20 km for sea sites in the available measurement data)

- Additional data sites should be concentrated in regions receiving signal paths through known or suspected anomalous propagation region(s) (e.g., San Joaquin Valley).

- Combination of land and sea data yields a higher accuracy calibrated grid than possible with land data alone.

Although the issue of utilizing land vs sea data has not been fully investigated due to limited quantity and spatial (coastal) coverage provided by the available sea calibration data, preliminary results indicate the following:

- Either land or sea data may be used to calibrate a CCZ grid

- Some sea data are always desired to identify land/sea interface effects

- Sea data collected over a wider coastal region will help to identify potential source(s) of the sea bias seen in the present study

- Both near and far from shore sea data will provide greater observability to sea model parameters (coefficients)

- Inclusion of land data greatly reduces the required density of sea calibration data as the dominant bearing dependence effects are easily observable in the land data.

It is recommended that additional sea data of the type described above be used to verify the above preliminary findings.

6. CONCLUSIONS AND RECOMMENDATIONS

6.1 CONCLUSIONS

The utility of semi-empirical techniques to accurately calibrate Loran-C grids in the CCZ has been demonstrated by applying these techniques to the West Coast Loran-C CCZ. In this region, current U.S. Coast Guard prediction procedures have been reported to result in significant charting errors (Ref. 10). The TASC-developed algorithm exhibits the following characteristics:

- RMS TD error of 0.42 μsec over the sea TD measurement data points <u>not used</u> in model calibration and 0.35 μsec over the data points <u>used</u> in model calibration
- RMS position error of less than 400 m in the Southern California CCZ -- <u>a factor of four improvement over the original charting procedures (Ref. 10)</u>
- Reasonably accurate TDs beyond the CCZ (where measurement data were not available for model calibration)
- Computationally simple (can be implemented on a hand-held electronic calculator similar to the HP-67)
- Cost effective since much less calibration data are required than for other known calibration procedures
- Can be easily extended to include data from other coverage regions as it becomes available.

In addition the results of this study show:

- Land data alone can be used to calibrate the West Coast CCZ grid with an rms TD error of approximately 0.8 μsec
- Inclusion of sea calibration data produces a factor of two improvement in the calibrated grid accuracy
- A uniform distribution of 50 percent of the available data (average spacing of 100-200 km) provides an rms CCZ grid accuracy of 0.40 μsec as compared to 0.35 μsec acheived with 100% of the available data.

<u>In summary, the semi-empirical TD grid calibration techniques have been shown to be both effective and efficient for developing accurate CCZ grid</u>.

6.2 RECOMMENDATIONS

It is recommended that semi-empirical grid calibration techniques using both land and sea calibration data be applied to other Loran-C chains and regions of the Coastal Confluence Zone to develop accurate TD grids. In particular, it is recommended that this technique be applied to develop accurate TD grids for:

- Great Lakes
- East Coast
- Gulf of Mexico.

Also, it is recommended that a grid calibration data collection and management program plan be established to

- Design data collection requirements for future semi-empirical grid calibration of Loran-C chains
- Develop procedures and methods for collecting the most useful data and only necessary data
- Provide a capability for on-line interaction with the data collection team to identify and verify "abnormal" data behavior
- Manage the collected data so as to provide reliable and efficient computer access to any set or subset of raw or processed data
- Develop data handling and analysis software.

The data collection and management program plan outlined above wil provide the U.S. Coast Guard with a cost-effective technique for semi-empirical Loran-C grid calibration and chart validation.

APPENDIX A

CALIBRATED TD GRID ALGORITHMS

A.1 INTRODUCTION

This appendix presents the TD grid algorithms for the two "finalist" calibration models, identified as the GRB model and LRB model. The GRB model has been selected as the West Coast TD grid calibration model. Table A.1-1 gives a computational guide to equations and tables that are required to compute TDs, which are presented in this appendix. The TD is the difference between the times-of-arrival of signals from the i^{th} secondary (w, x or y) and master (m) stations at a user as illustrated in Fig. A.1-1 and expressed by the following equation:

$$TD_i = (T_i - T_m) + (SF_i - SF_m) + \overline{ED}_i + b_i \qquad (A.1\text{-}1)$$

where

$$T_i = \frac{n\ R_i}{c}\ \mu sec \qquad (A.1\text{-}2)$$

$$T_m = \frac{n\ R_m}{c}\ \mu sec \qquad (A.1\text{-}3)$$

R_i = i^{th} secondary station-to-user great-circle path length

R_m = master station-to-user great-circle path length

TABLE A.1-1
TD COMPUTATION GUIDE

<table>
<tr><td colspan="4">TD Equation: $TD_i = T_i - T_m + SF_i - SF_m + \overline{ED}_i + b_i$</td></tr>
<tr><th colspan="2">TD EQUATION TERMS</th><th>EQUATION NUMBER</th><th>TABLE NUMBER</th></tr>
<tr><td colspan="2">T_i</td><td>A.1-2</td><td>-</td></tr>
<tr><td colspan="2">T_m</td><td>A.1-3</td><td>-</td></tr>
<tr><td rowspan="6">$SF_i = SF_j\big|_{j=i}$
$SF_j = \frac{1}{2}[-S_1+S_2+S_3-S_4+S_5+S_6]$
$SF_m = SF_j\big|_{j=m}$</td><td>S_1</td><td>A.3-1</td><td>-</td></tr>
<tr><td>S_2</td><td>A.3-2</td><td>A.3-1</td></tr>
<tr><td>S_3</td><td>A.3-3</td><td>A.3-1</td></tr>
<tr><td>S_4</td><td>A.3-4</td><td>A.3-1</td></tr>
<tr><td>S5</td><td>A.3-6</td><td>A.3-2</td></tr>
<tr><td>S_6</td><td>A.3-7</td><td>A.3-2</td></tr>
<tr><td rowspan="3">$\overline{ED}_i$</td><td>$\overline{ED}_w$</td><td>A.1-4</td><td>-</td></tr>
<tr><td>$\overline{ED}_x$</td><td>A.1-5</td><td>-</td></tr>
<tr><td>$\overline{ED}_y$</td><td>A.1-6</td><td>-</td></tr>
<tr><td colspan="2">b_i</td><td>-</td><td>A.2-1</td></tr>
</table>

c = speed of light in a vacuum
= 2.99792458×10^8 m/sec

n = surface refractive index
= 1.000338

$\overline{ED}_w$ = 13796.90 μsec (A.1-4)

$\overline{ED}_x$ = 28094.50 μsec (A.1-5)

$\overline{ED}_y$ = 41967.30 μsec (A.1-6)

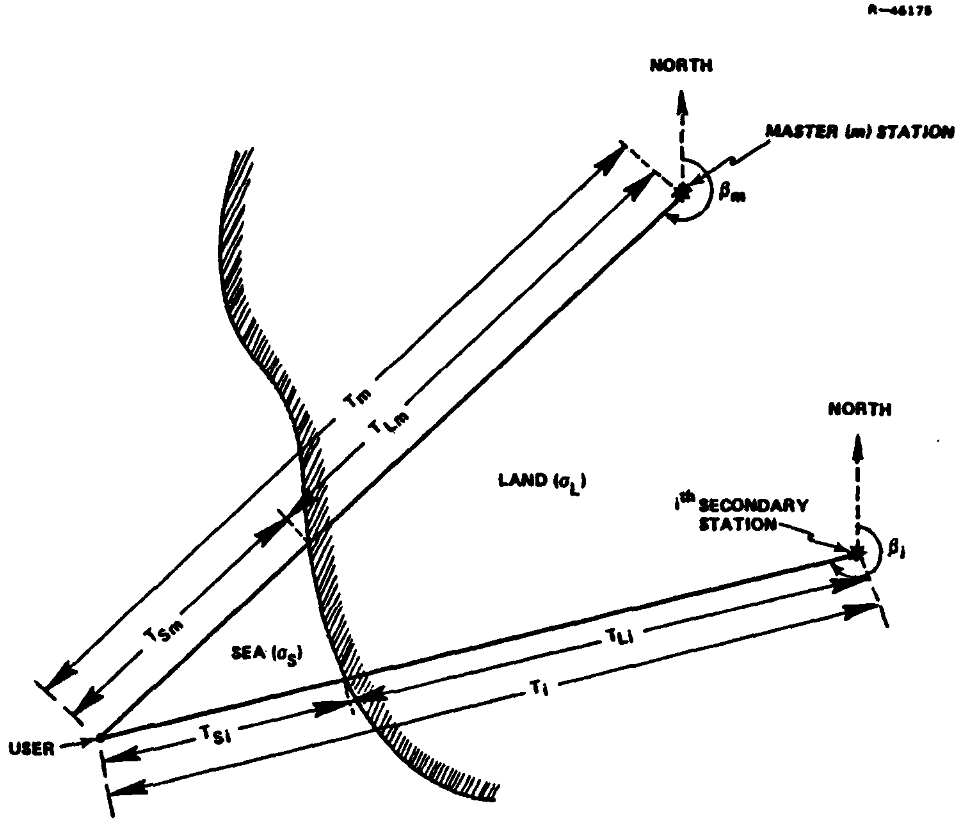

Figure A.1-1   Mixed Path TD Geometry

SF_i = Secondary Phase Delay* (SF) from i^{th} secondary station-to-user (μsec)

SF_m = Secondary Phase Delay* (SF) from master (m) station-to-user (μsec)

b_i = TD bias associated with the i^{th} secondary station (μsec)

Note, ED_i (i = w, x or y) is the published emission delay at the i^{th} secondary station (Ref. 1). The calibrated values of the TD biases, b_i, for the GRB and LRB models are given in Table A.1-2.

---

*Throughout this report, SF denotes the total secondary phase delay of the groundwave signal propagating over any land and/or water path.

The numerical values of TD biases are different for each model and each TD component (i.e., TDW, TDX or TDY). In addition, land (i.e., all-land), and mixed (i.e., land/sea water), TD paths use different values for the TD bias, as tabulated in Table A.1-2. The biases presented in Table A.1-2 apply when both station signal paths forming a TD are either land or mixed.

TABLE A.1-2

CALIBRATED TD BIASES FOR GRB AND LRB MODELS

TD COMPONENT	TD BIAS - μsec			
	STATION-TO-SITE SIGNAL PATH			
	LAND		MIXED	
	GRB	LRB	GRB	LRB
TDW	-0.854	-0.394	*	*
TDX	-1.648	-0.262	-1.173	-0.425
TDY	0.085	0.294	-0.353	-0.470

*Available to estimate mixed path TD bias for TDW.

Formulas to compute a mixed path SF from land and sea water path SFs are given in Section A.2. The calibrated algorithms for the SFs of the GRB and LRB models are presented in Section A.3. The measured, computed and residual TDs at the TD measurement data sites, obtained with the GRB model, are given in Section A.4.

A.2 MIXED PATH SF EQUATION

Using Millington's method (Eqs. 2.2-1 through 2.2-3), the formula for a mixed path SF from the j^{th} (= w, x, y or m) station to a user is

$$SF_j = \frac{1}{2}\left[\overbrace{SF_L(T_j,\beta_j)}^{S_5} + \overbrace{SF_L(T_{Lj},\beta_j)}^{S_6} - \overbrace{SF_L(T_{Sj})}^{S_1} + \underbrace{SF_S(T_j)}_{S_2} + \underbrace{SF_S(T_{Sj})}_{S_3} - \underbrace{SF_S(T_{Lj})}_{S_4}\right] \mu sec \qquad (A.2\text{-}1)$$

where $SF_L(T,\beta)$ is the SF of a land path of length T (μsec) and bearing angle β^* at the station; and $SF_S(T)$ is the SF of a sea water path of length T. In general, the functions SF_L and SF_S may be station specific. The path lengths T_{Lj}, T_{Sj}, T_j in Eq. A.2-1 refer to the land segment, sea segment and total length, of a signal path from the j^{th} station to a user, respectively. Section A.3 gives formulas to compute each of the six terms included in Eq. A.2-1.

A.3 EQUATIONS OF MIXED PATH SF COMPONENTS

A.3.1 Term S_1

The term S_1 in Eq. A.2-1 is the SF of a land path of length T_{Sj} (μsec) from the j^{th} station and is given by

$$S_1 = SF_L(T_{Sj})$$

$$= \frac{0.795}{T_{Sj}} + 0.439 + 0.00245\, T_{Sj}\ \mu sec \qquad (A.3\text{-}1)$$

Note, for an all-land or all-sea water path, S_1 is zero.

---

*Term S_1 in Eq. A.2-1 does not depend on the bearing angle.

A.3.2 Terms S_2, S_3 and S_4

Terms S_2, S_3 and S_4 in Eq. A.2-1 are the SFs for sea water path lengths T_j, T_{Sj} and T_{Lj}, respectively. The sea SF model associated with both the GRB and LRB models depends only on range to the station in the following manner:

$$S_2 = SF_S(T_j) \tag{A.3-2}$$

$$S_3 = SF_S(T_{Sj}) \tag{A.3-3}$$

$$S_4 = SF_S(T_{Lj}) \tag{A.3-4}$$

where the sea water SF for a path of length T (μsec) is given by

$$SF_S(T) = \begin{cases} \frac{a_{-1}}{T} + a_o + a_1 T \ \mu\text{sec}, & \text{if } 10 \leq T \leq 540 \ \mu\text{sec} \\ \frac{a'_{-1}}{T} + a'_o + a'_1 T \ \mu\text{sec}, & \text{if } T \geq 540 \ \mu\text{sec} \end{cases} \tag{A.3-5}$$

The calibrated values of the sea coefficients associated with the GRB and LRB models are given in Table A.3-1. Note, for an all-land path, the terms S_2, S_3 and S_4 are each zero; for an all-sea water path, however, only the term S_4 is zero.

A.3.3 Terms S_5 and S_6

Terms S_5 and S_6 in Eq. A.2-1 are the SFs of land paths of lengths T_j and T_{Lj}, respectively. In both the GRB and LRB models, these terms include bearing angle dependence in addition to the range dependence. Terms S_5 and S_6 are given below by SFs associated with a land path of length T_j (μsec) and subtending a bearing angle of β_j (measured positive clockwise from north) at the j^{th} station:

TABLE A.3-1

CALIBRATED VALUES OF SEA SF MODEL COEFFICIENTS FOR GRB AND LRB MODELS

COEFFICIENT	MODEL	
	GRB	LRB
a_{-1}	3.188	2.885
a_o	-0.594	-0.387
a_1	0.000329	0.000332
a'_{-1}	128.8	130.4
a'_o	0.187	-0.012
a'_1	0.000652	0.000660

$$S_5 = SF_L(T_j, \beta_j) \quad (A.3\text{-}6)$$

$$S_6 = SF_L(T_{Lj}, \beta_j) \quad (A.3\text{-}7)$$

where the formulas for the SF_L of a land path of length T_j (μsec) and bearing β_j (deg) for the GRB and LRB models are given by

GRB Model:

$$SF_L(T_j, \beta_j) = A_o + A_1 T_j + \sum_{\ell=1}^{2} [C_{j\ell} \sin \ell\beta_j + D_{j\ell} \cos \ell\beta_j] \quad \mu sec$$

(A.3-8)

LRB Model:

$$SF_L(T_j, \beta_j) = A_o + [A_1 + B_1 f_j(\beta_j)] T_j \quad \mu sec \quad (A.3\text{-}9)$$

The function $f_j(\beta_j)$ is zero for j = m,w and y. However, $f_j(\beta_x)$ is unity for bearing angles between 3 and 150 deg and zero for

all other bearing angles. Calibrated coefficient values of the GRB and LRB models, Eqs. A.3-8 and A.3-9, are as given in Table A.3-2.

TABLE A.3-2

CALIBRATED VALUES OF LAND SF MODEL COEFFICIENTS FOR GRB AND LRB MODELS

COEFFICIENTS	MODEL	
	GRB	LRB
A_o	1.428†	1.428†
A_1	0.00158	0.00156
B_1	*	-0.00067
C_{w1}	0	
C_{w2}	-0.711	
D_{w1}	0.323	
D_{w2}	0	
C_{x1}	0	
D_{x1}	0	
C_{x2}	0	
D_{x2}	0.942	*
C_{y1}	0	
D_{y1}	0	
C_{y2}	0.588	
D_{y2}	0	
C_{m1}	1.010	
C_{m2}	-0.196	
D_{m1}	-0.893	
D_{m2}	-0.355	

*Not Applicable.

†Theoretical Values (unobservable from the calibration data).

A.4 COMPUTED TDs AT CALIBRATION DATA SITES

Tables A.4-1 and A.4-2 present the measured and computed TDs, and TD residuals at the land and sea calibration data sites, respectively. The computed TDs and the residuals were obtained with the GRB model which has been selected as the West Coast Grid calibration model (see Chapter 4). (Note, Fig. 4.4-1 shows plots of the site residuals tabulated in Tables A.4-1 and A.4-2.)

TABLE A.4-1

MEASURED, CALIBRATED AND RESIDUAL TIME DIFFERENCES AT LAND DATA SITES (GRB MODEL)

T-3547

TASC SITE IDENTI-FICATION	TIME DIFFERENCE - μsec								
	TDW			TDX			TDY		
	MEASURED	CALIBRATED	RESIDUAL	MEASURED	CALIBRATED	RESIDUAL	MEASURED	CALIBRATED	RESIDUAL
1	11297.483	11297.795	-0.312	28211.939	28211.751	0.188	43850.462	43850.632	-0.170
2	11395.015	11395.229	-0.214	28228.481	28228.627	-0.146	0.000	43852.695	
3	11919.090	11918.802	0.288	28079.418	28079.364	0.054	43907.798	43907.756	0.042
4	12075.060	12074.891	0.169	28054.780	28054.069	0.711	0.000	43915.476	
5	12078.347	12078.194	0.153	28054.795	28054.274	0.521	43915.396	43915.509	-0.113
6	12616.235	12616.333	-0.098	28114.235	28114.675	-0.440	43915.660	43915.571	0.089
7	12913.894	12914.114	-0.220	27984.928	27984.739	0.189	43933.169	43934.087	-0.918
8	13514.290	13514.170	0.120	27801.215	27800.752	0.463	43931.437	43931.233	0.204
9	13679.803	13679.937	-0.134	27742.524	27741.917	0.607	43923.179	43922.895	0.284
10	14353.579	14353.970	-0.391	27573.528	27573.955	-0.427	43872.846	43872.681	0.165
11	15164.430	15164.751	-0.321	27723.896	27725.733	-1.837	43859.591	43859.593	-0.002
12	15179.554	15179.052	0.502	27291.878	27291.807	0.071	43725.263	43725.152	0.111
13	15410.009	15409.511	0.498	27225.781	27225.559	0.222	43673.367	43673.432	-0.065
14	15618.499	15618.029	0.470	27067.188	27066.944	0.244	43560.515	43560.807	-0.292
15	0.000	15864.975		26997.864	26997.600	0.264	0.000	43492.132	
16	15946.970	15946.810	0.160	27084.290	27084.052	0.238	43290.030	43290.030	-0.000
17	16091.059	16091.204	-0.145	27242.118	27242.423	-0.305	43199.210	43198.825	0.385
18	16133.682	16134.057	-0.375	27289.521	27290.014	-0.493	43121.187	43120.766	0.421
19	16358.456	16358.936	-0.480	27596.470	27596.958	-0.488	42698.504	42698.466	0.038
20	16300.899	16301.259	-0.360	27493.970	27494.319	-0.349	42756.410	42756.208	0.202
21	16475.055	16475.248	-0.193	27795.923	27795.821	0.102	42318.706	42319.063	-0.357
22	16483.635	16483.822	-0.187	27779.325	27779.107	0.218	42118.129	42118.112	0.017
27	16561.713	16561.613	0.100	27967.883	27967.133	0.750	41611.644	41611.647	-0.003
30	16595.832	16595.701	0.131	28228.679	28228.787	-0.108	41116.852	41117.268	-0.416
39	16570.525	16569.985	0.540	28391.094	28391.024	0.070	40593.120	40593.953	-0.833
43	16592.861	16592.561	0.300	28250.499	28250.958	-0.459	40812.136	40811.902	0.234
50	0.000	16582.266		28288.773	28288.633	0.140	40539.830	40538.851	0.979

TABLE A.4-2

MEASURED, CALIBRATED AND RESIDUAL TIME DIFFERENCES AT SEA DATA SITES (GRB MODEL)

T-3548

TASC SITE IDENTI-FICATION	TIME DIFFERENCE - μsec					
	TDX			TDY		
	MEASURED	CALIBRATED	RESIDUAL	MEASURED	CALIBRATED	RESIDUAL
23	27808.800	27808.702	0.098	41916.000	41915.664	0.336
24	27801.100	27800.991	0.109	41920.000	41919.625	0.375
25	27913.400	27913.421	-0.021	41698.300	41698.198	0.102
26	27835.700	27835.474	0.226	41796.300	41796.295	0.005
28	27976.400	27976.117	0.283	41592.400	41592.217	0.183
29	27880.300	27879.904	0.396	41699.000	41698.899	0.101
31	27965.400	27965.311	0.089	41548.000	41548.389	-0.389
32	28036.200	28035.377	0.823	41410.500	41410.958	-0.458
33	27896.000	27896.202	-0.202	41615.700	41616.141	-0.441
34	28094.900	28094.947	-0.047	41294.500	41294.593	-0.093
35	28062.800	28062.670	0.130	41339.100	41339.212	-0.112
36	28002.900	28002.263	0.637	41419.400	41419.384	0.016
37	28165.400	28166.067	-0.667	41122.500	41122.761	-0.261
38	27976.600	27976.187	0.413	41450.900	41450.946	-0.046
40	28174.400	28174.928	-0.528	41036.000	41036.355	-0.355
41	28199.200	28199.780	-0.580	40981.300	40981.494	-0.194
42	28244.100	28244.715	-0.615	40846.100	40845.359	0.741
44	28273.500	28273.992	-0.492	40675.300	40674.968	0.332
45	28120.400	28120.164	0.236	40975.600	40975.886	-0.286
46	28271.900	28272.205	-0.305	40638.200	40637.741	0.459
47	28097.400	28097.456	-0.056	40974.300	40974.495	-0.195
48	28262.800	28262.782	0.018	40601.000	40600.777	0.223
49	28227.400	28227.345	0.055	40674.000	40674.043	-0.043

REFERENCES

1. Warren, R.S., Gupta, R.R., and Healy, R.D., "Design and Calibration of a Grid Prediction Algorithm for the St. Marys River Loran-C Chain," The Analytic Sciences Corporation, Technical Information Memorandum TIM-1119-2, March 1978.

2. Roland, W. (Editor), Wild Goose Association Radionavigation Journal, Wild Goose Association, Inc., Acton, MA, 1976.

3. Gelb, A. (Editor), Applied Optimal Estimation, M.I.T. Press, Cambridge, 1974.

4. Johler, J.R., Keller, W.J., and Walters, L.C., "Phase of the Low Radio Frequency Ground Wave," National Bureau of Standards Cicular 573, June 1956.

5. Millington, G., "Ground Wave Propagation over an Inhomogeneous Smooth Earth," Proceedings of the Institute of Electrical Engineers, Vol. 96, Pt. III, January 1949.

6. Hufford, G.A., "An Integral Equation Approach to the Problem of Wave Propagation over an Irregular Surface," Quarterly Journal of Applied Math., Vol. 9, No. 4, 1952.

7. Gupta, R.R., "Groundwave Signal Prediction Techniques," The Analytic Sciences Corporation, Technical Information Memorandum TIM-735-3, July 1976.

8. Illegen, J.D., and Feldman, D.A., "Loran-C Signal Analysis Experiments, 'An Overview'," Proc. of the Seventh Annual Technical Symposium of the Wild Goose Association (New Orleans, La), October 1978.

9. Uttam, B., "Loran-C Additional Secondary Phase Factor (ASF) Correction Algorithm," The Analytic Sciences Corporation, Technical Report TR-735-1, October 1976.

10. Doherty, R.H., and Johler, J.H., "Interpretation of West Coast Loran-C Spatial Errors Using Programmable Calculator Analysis Techniques," Proc. of the Seventh Annual Technical Symposium of the Wild Goose Association (New Orleans, La), October 1978.